WL-TR-94-4100

CREEP RESISTANT OXIDE FIBERS

John W. Halloran, Richard M. Laine,
Bruce H. King, and Yin Liu

University of Michigan
Department of Engineering
Ann Arbor, MI 48109-2136

March 1994

Final Report for Period 21 August 1991 - 21 November 1993

MATERIALS DIRECTORATE
WRIGHT LABORATORY
AIR FORCE MATERIEL COMMAND
WRIGHT-PATTERSON AFB OH 45433-7734

NOTICE

WHEN GOVERNMENT DRAWINGS, SPECIFICATIONS, OR OTHER DATA ARE USED FOR ANY PURPOSE OTHER THAN IN CONNECTION WITH A DEFINITELY GOVERNMENT-RELATED PROCUREMENT, THE UNITED STATES GOVERNMENT INCURS NO RESPONSIBILITY OR ANY OBLIGATION WHATSOEVER. THE FACT THAT THE GOVERNMENT MAY HAVE FORMULATED OR IN ANY WAY SUPPLIED THE SAID DRAWINGS, SPECIFICATIONS, OR OTHER DATA, IS NOT TO BE REGARDED BY IMPLICATION OR OTHERWISE IN ANY MANNER CONSTRUED, AS LICENSING THE HOLDER OR ANY OTHER PERSON OR CORPORATION, OR AS CONVEYING ANY RIGHTS OR PERMISSION TO MANUFACTURE, USE, OR SELL ANY PATENTED INVENTION THAT MAY IN ANY WAY BE RELATED THERETO.

THIS REPORT IS RELEASABLE TO THE NATIONAL TECHNICAL INFORMATION SERVICE (NTIS). AT NTIS, IT WILL BE AVAILABLE TO THE GENERAL PUBLIC, INCLUDING FOREIGN NATIONS.

THIS TECHNICAL REPORT HAS BEEN REVIEWED AND IS APPROVED FOR PUBLICATION.

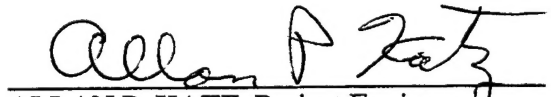

ALLAN P. KATZ, Project Engineer
Materials Development Branch
Metals and Ceramics Division

GERALD J. PETRAK, Actg Chief
Materials Development Branch
Metals and Ceramics Division

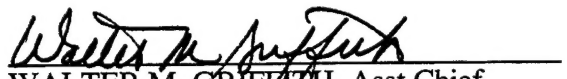

WALTER M. GRIFFITH, Asst Chief
Metals and Ceramics Division
Materials Directorate

IF YOUR ADDRESS HAS CHANGED, IF YOU WISH TO BE REMOVED FROM OUR MAILING LIST, OR IF THE ADDRESSEE IS NO LONGER EMPLOYED BY YOUR ORGANIZATION, PLEASE NOTIFY, WL/MLLM, WRIGHT-PATTERSON AFB OH 45433-7817 TO HELP US MAINTAIN A CURRENT MAILING LIST.

COPIES OF THIS REPORT SHOULD NOT BE RETURNED UNLESS RETURN IS REQUIRED BY SECURITY CONSIDERATIONS, CONTRACTUAL OBLIGATIONS, OR NOTICE ON A SPECIFIC DOCUMENT.

DISCLAIMER NOTICE

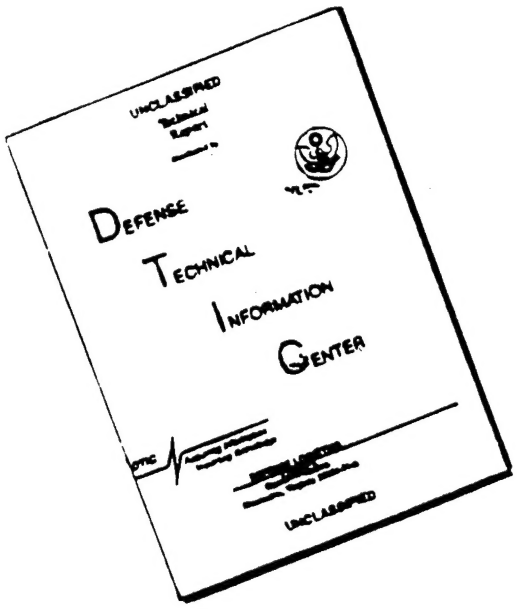

THIS DOCUMENT IS BEST QUALITY AVAILABLE. THE COPY FURNISHED TO DTIC CONTAINED A SIGNIFICANT NUMBER OF PAGES WHICH DO NOT REPRODUCE LEGIBLY.

REPORT DOCUMENTATION PAGE

FORM APPROVED
OMB NO. 0704-0188

1. AGENCY USE ONLY (Leave blank)	2. REPORT DATE	3. REPORT TYPE AND DATES COVERED
	March 1994	Final Report for 21 Aug 1991 - 21 Nov 1993

4. TITLE AND SUBTITLE

Creep Resistant Oxide Fibers

5. FUNDING NUMBERS

C - F33615-91-C-5650
PE - 62102F
PR - 2420
TA - 01
WU - 94

6. AUTHOR(S)

John W. Halloran, Richard M. Laine, Bruce H. King, and Yin Liu

7. PERFORMING ORGANIZATION NAMES(S) AND ADDRESS(ES)

University of Michigan
Department of Engineering
Ann Arbor, MI 48109-2136

8. PERFORMING ORGANIZATION REPORT NUMBER

9. SPONSORING/MONITORING AGENCY NAMES(ES) AND ADDRESS(ES)

Materials Directorate
Air Force Wright Laboratory, AFMC
Wright-Patterson AFB OH 45433-7734

10. SPONSORING/MONITORING AGENCY REPORT NUMBER

WL-TR-94-4100

11. SUPPLEMENTARY NOTES

12a. DISTRIBUTION/AVAILABILITY STATEMENT

Approved for public release, distribution is unlimited.

12b. DISTRIBUTION CODE

A

13. ABSTRACT (Maximum 200 words)

Yttrium aluminate garnet ("YAG" - $Y_3Al_5O_{12}$) fibers were fabricated by two methods: a sol-gel method and a carboxylate precursor method. Both methods yielded fine diameter fibers of dense, phase-pure YAG. Green fibers were continuously spun from the sol-gel system and the carboxylate systems. Sintering was done in a batch mode. The sol-gel fibers were fabricated from commercial oxide colloidal sols, mixed with water-soluble polymers. The sintered YAG fibers had excellent bend stress relaxation (BSR) creep resistance. The BSR creep temperature for the YAG fibers was increased by 220°C over DuPont's alumina-based PRD 166 fibers and 275°C over DuPont's Fiber FP alumina fibers. The room temperature strength of the sol-gel YAG fibers was 500-700 MPa, limited by processing defects. The fabrication, spinning, sintering, and YAG phase development are reported in detail. The carboxylate precursor methods led to phase pure YAG fibers with fine diameters. Several promising systems were explored. Solutions of yttrium and aluminum isobutyrates, in THF, were readily spinnable. These could be pyrolyzed and snitered into dense YAG fibers under correct conditions. Aqueous formoacetate dopes were also developed, using yttrium formate and aluminum acetate mixtures. These also spun well, and could yield dense YAG.

14. SUBJECT TERMS

Oxide fibers, creep, YAG

15. NUMBER OF PAGES

55

16. PRICE CODE

17. SECURITY CLASSIFICATION OF REPORT	18. SECURITY CLASSIFICATION OF THIS PAGE	19. SECURITY CLASSIFICATION OF ABSTRACT	20. LIMITATION OF ABSTRACT
Unclassified	Unclassified	Unclassified	Unlimited

TABLE OF CONTENTS

LIST OF FIGURES

LIST OF FIGURES (continued)

LIST OF TABLES

SUMMARY

Yttrium aluminate garnet ("YAG"-$Y_3Al_5O_{12}$) fibers were fabricated by two methods: a sol-gel method and a carboxylate precursor method. Both methods yielded fine diameter fibers of dense, phase-pure YAG. Green fibers were continuously spun from the sol-gel system and the carboxylate systems. Sintering was done in a batch mode.

The sol-gel fibers were fabricated from commercial oxide colloidal sols, mixed with water-soluble polymers. The sintered YAG fibers had excellent bend stress relaxation (BSR) creep resistance. The BSR creep temperature for the YAG fibers was increased by 220°C over DuPont's alumina-based PRD 166 fibers and 275°C over DuPont's Fiber FP alumina fibers. The room temperature strength of the sol-gel YAG fibers was 500-700 MPa, limited by processing defects. The fabrication, spinning, sintering, and YAG phase development are reported in detail.

The carboxylate precursor methods lead to phase pure YAG fibers with fine diameters. Several promising systems were explored. Solutions of yttrium and aluminum isobutyrates, in THF, were readily spinnable. These could by pyrolyzed and sintered into dense YAG fibers under correct conditions. Aqueous formoacetate dopes were also developed, using yttrium formate and aluminum acetate mixtures. These also spun well, and could yield dense YAG.

A second and more ambitious goal was to achieve in the YAG fibers a more creep resistant microstructure by producing axially elongated YAG grains. This was not achieved, precluding the opportunity to test hypotheses on methods to create elongated grains.

1. INTRODUCTION

Advanced oxide fibers with creep resistance at or above 1350°C are needed for ceramic matrix composites for use in oxidizing atmospheres. Yttrium aluminum garnet, $Y_3Al_5O_{12}$, (YAG) is an attractive material by virtue of its high melting point and exceptionally low dislocation climb-limited creep rate[1]. YAG ceramic fibers are not currently available, so the major goal of this project was the development of creep resistant yttrium aluminum garnet fibers. This was accomplished, and we produced equiaxed YAG fibers by a sol-gel method with excellent bend stress relaxation (BSR) creep resistance. The BSR creep temperature for the YAG fibers was increased by 220°C over PRD 166 fiber and 275°C over Fiber FP alumina fibers. The strength of these YAG fibers was limited by processing defects to about 500-700 MPa. This report will present the properties and processing of the sol-gel fibers in Section 2. A second fabrication method, using carboxylate precursors, led to phase pure YAG fibers from several promising systems, including isobutyrates, formoacetates, and formates. We present the synthesis and properties of the carboxylate YAG fibers in Section 3.

A second and more ambitious goal was to achieve in the YAG fibers a more creep resistant microstructure, which could enable significantly better creep resistance than polycrystalline alumina of comparable grain size[2]. We attempted to produce creep-resistant YAG fibers with axially elongated grains, with the hope that this would suppress diffusional creep as it does with tungsten incandescent lamp filaments. The excellent creep resistance of tungsten filaments arises from its long-grain interpenetrating grain structure.[3] This grain structure is created during W wire fabrication by rows of tiny bubbles along the wire axis, which constrain radial grain growth and promote axial grain growth during recrystallization, so the unique long interlocking grains develop.[4] Our strategy was to conduct a directional recrystallization in fibers having an axially-aligned second phase of alumina. This structure was to be produced by simultaneously spinning two unmixed streams of YAG dope and alumina dope. Spinning two streams together is known as "bicomponent spinning" in the fiber field[5], and can be achieved with well-designed spinning dies using two dopes with appropriate rheological behavior. Despite much effort and encouraging progress, we did not achieve effective bicomponent spinning with our precursors, so could not test the concept of directional recrystallization via axially aligned second phases. Work continued on this problem until the end of the project.

This research was conducted as two related Masters thesis projects. The original plan was for Mr. Yin Liu to synthesize and characterize a carboxylate precursor dope and conduct small-scale fiber spinning. Mr. Bruce King would use Liu's precursors, spin continuous fibers with a goal for bicomponent spinning. King would be responsible for mechanical testing. This was an aggressive plan which relied on very fast development of precursors. Precursor development proved to be more time consuming. Also, during the early stages of the project, before carboxylate dopes were available in quantity, Bruce King developed a sol-gel method for YAG fibers. The sol-gel fibers were quite attractive, and it seemed that the goal of bicomponent spinning

could be reached faster with sol-gel dopes. King continued to work on the sol-gel system.

This report combines the results of the King MS thesis on processing and characterization of YAG fibers by a colloidal sol-gel method, and the Liu MS thesis on synthesis, pyrolysis, and fiber spinning of isobutyrate and formoacetate YAG precursors. At the time of this writing, both theses are being completed. They will provide a more detailed presentation and analysis of these results. This report will summarize the important activities and major results for this project.

2. SOL-GEL FIBERS

The sol-gel YAG fibers were fabricated using a quite simple approach which differs from the previously reported alkoxide methods[6]. It involved relatively simple mixing of two commercial colloids in a water-soluble polymer. For the yttria, a 14 weight percent dispersion of 10 nm Y_2O_3 particles (Nyacol Colloidal Yttria, Nyacol Products, Ashland, MA) was used. The source of the alumina was a 20 weight percent dispersion of 50 nm AlOOH (Al-20, Nyacol Products, Ashland, MA). Dope processing was done in air, using simple mixers and dryers, and common polymers. The green fibers could be fired in air directly to the sintering temperature, avoiding elaborate heating schedules. This method has potential for low-cost YAG fiber due to the simple processing and relatively inexpensive oxide raw materials. The February 1994 cost of these materials are $0.96/lb for the alumina sol and $14.85/lb for the yttria sol, which leads to raw material cost of $62.50/lb for dry YAG.

Production of YAG fibers from colloidal sols involved many interrelated steps. The largest problems encountered were with the processing of the raw materials into a homogeneous, spinnable dope, and as a result, most of the work performed was devoted to this. Ultimately, it was possible to spin long lengths of green fiber which could be fired to give dense YAG. Unfortunately, this stage was not reached until late in the project, resulting in little feedback from the mechanical testing and creep experiments. It is thought that further refinements of the dope processing step will bring about substantial increases in the mechanical properties of YAG fibers produced by this method.

2.1. Sol-Gel Processing

With a sol-gel approach, concentration of the sol often results in the development of a gel network which is suitable for spinning . This is especially true of alkogels, where the metal ions are contained in a polymer chain. However, the gel network which develops from colloidal sols is due to electrostatic interactions and is easily destroyed by the large shear to which the fluid is exposed during spinning. For this reason, spinning aids are often added to colloidal sols to render them spinnable. This was the case with the sol system selected for this investigation. The sols, as received, were stabilized electrostatically at pH 7 (yttria) and pH 4.4 (hydrous alumina). They coagulated quickly when mixed. Attempts to stabilize the two at a common pH proved unsuccessful, necessitating the use of colloidal stabilizers to produce homogenous mixtures. Many of the water soluble binders available as spinning aids are also effective colloidal stabilizers. Binder selection thus focused on both of these aspects in an attempt to keep the system as simple as possible.

Concentration of the dopes to a spinnable rheology turned out to be a non-trivial task. It was found that the solvent evaporation rate was much faster than the solvent diffusion rate through the concentrated dopes, leading to skin formation. Presence of this dried material in the dope destroyed homogeneity, leading to processing defects

and spin line fracture. Although most of the concentration techniques which were explored exhibited other problems as well, achieving a homogenous dope was a critical aspect of forming sound fibers. In relation to this, it was necessary to be able to determine the water content of dopes for reproducibility.

Dope processing therefore focused on binder selection, determination of techniques to control water concentration/dope viscosity and finally, determination of the appropriate water concentration to render the dope spinnable. None of these aspects of processing were independent of one another. It was often found that solutions to one problem solved another. In a like manner, solutions to a problem often dictated that changes be made in another aspect of processing.

2.1.1. Binder Selection

Binder selection involved the identification of a polymer which was compatible with the colloidal sol system. Water solubility, low ash yield, stability over a range of pH, and ability to act as a colloidal stabilizer were all important considerations. Examination of the fiber spinning literature identified polyvinyl pyrrolidinone (PVP) and polyethylene oxide (PEO) as commonly used spinning aids.

PVP: Two grades of PVP were investigated; K-30 (molecular weight = 40,000) and K-90 (m.w. = 360,000) supplied by GAF. Neat solutions of each were found to be hand spinnable. Preliminary firing experiments with short lengths of fiber spun with K-90 showed that binder burnout was not a problem, as green fibers could be heated very quickly to high temperature with no evidence of bloating or cracking due to gas evolution. Furthermore, achieving dense fibers did not appear to be a problem.

PEO: Several grades of PEO were investigated, as it is available in molecular weights ranging from 100 (Carbowax PEG-100) to 8,000,000 (Polyox WSR-308), all supplied by Union Carbide. The lower molecular weight grades (<20,000) are referred to as polyethylene glycol (PEG), but the chemical formula is the same as PEO. This wide range of molecular weights made custom tailoring of polymer blends possible, an aspect which became critical for achieving a balance between spinnability and colloidal stability. PEG is a liquid (grades 100 - 600) or waxy solid (grades 900-20M) and was used only in colloidal stabilization experiments. Neat water solutions of all Polyox grades attempted (WSR N-10, N-80, N-750, WSR-205, 301 and 303) are hand spinnable, and high molecular weight versions exhibit hand-spinnability at concentrations as low as 1 wt.% in water. As with PVP, no problems were encountered in firing short segments of fibers.

2.1.2. Stability of Mixed Sols

As was mentioned above , simple mixing of the two colloidal sols resulted in rapid coagulation. This was not surprising, since the sols were stabilized at different pH values as received, Y_2O_3 at 7.0 and Al_2O_3 at 4.0. Attempts to stabilize the two at a common pH proved fruitless, however addition of polymer was found to reduce the

scale of coagulation. Phase development studies (Section 2.3.2.) showed that a series of intermediate phases formed prior to YAG during reaction of the sols. These phases reacted to form phase pure YAG below 1500°C in powders from homogeneous dopes, however large quantities of these intermediate phase remained in powders from inhomogeneous dopes even after repeated firings to temperatures above 1500°C. Powders from inhomogeneous dopes containing polymers were found to contain a single intermediate phase, $YAlO_3$ perovskite (YAP), thus the presence of YAP at 1500°C was taken as an indicator of the degree of colloidal stabilization (and hence dope homogeneity) provided by the polymer. Powder XRD was used to detect and quantify the presence of YAP.

In general, it was found that increasing the polymer concentration in the dope decreased the amount of retained YAP, indicating a higher degree of sol stabilization. This was first observed in dopes prepared using PEG 20M (m.w. =20,000) as a binder. However, as much as 50 wt% binder was required to substantially lower the amount of retained YAP. The use of higher molecular weight PEO reduced the amount of binder needed while still providing effective stabilization, however, there was a practical limit to this. The very high molecular weight grades (>1,000,000) of PEO are known to act as coagulants rather than stabilizers due to bridging flocculation. This was indeed the case for fibers spun using PEO WSR-303 (m.w. = 7,000,000). Although the dopes were macroscopically homogeneous, YAP was always present in fibers spun using a variety of concentrations of WSR-303. WSR-205, on the other hand, was found to be very effective at providing colloidal stabilization.

The homogeneity of dopes containing PVP were found to be strongly influenced by the order of addition of the various components. PVP tended to form a lumpy mass when added directly to the alumina sol, but this behavior was not observed in the yttria sol. PVP dopes were thus prepared by first adding PVP to the yttria sol, then adding the alumina sol to this. It was found that the rate of alumina sol addition affected homogeneity, so the alumina sol was titrated into the yttria-PVP mixture which was being stirred vigorously. This method produced the most homogenous PVP-based dopes.

Sol homogeneity was found to be influenced by several factors other than the polymer. Heating above 70°C-80°C resulted in coagulation which was visible, while the shearing action of fiber spinning was found to homogenize the dope. These results had dramatic affects on the processing for very practical reasons. Since the maximum temperature to which the dilute sol could safely be heated was limited to 50°C-60°C, concentration was a slow process. The greater homogeneity achieved during spinning relaxed the stabilization requirements of the polymer.

2.1.3. Concentration Methods

Concentrating the dope to a high enough viscosity to spin while still maintaining homogeneity was not a straightforward task. Much of the work on concentration was by trial and error, thus inferior techniques were abandoned quickly once a superior

method was determined. Two basic approaches were used; evaporation of water from a dilute dope, and rehydration of powders obtained from a fully dried dope. The first approach could be used to concentrate dopes made with both PVP and PEO, while the second method worked only with PEO.

Several variations on evaporation were attempted. In all cases, water concentration was measured by monitoring weight loss during evaporation. The first method involved simple concentration on a hot plate while stirring, a technique which has been used in our laboratory with much success for preparing dry-spinning dopes of other systems. Coagulation of the sols occurred on heating above 70°C - 80°C, limiting the temperature to approximately 50°C and resulting in an extremely slow concentration rate. Furthermore, once the dope viscosity increased appreciably, the stir bar ceased to spin and a crust formed on the surface. Application of a vacuum to speed up concentration resulted in a slight improvement over the hot plate alone, but led to other problems. The dope was first heated on a hot plate, then placed in a vacuum chamber which was pumped by a mechanical pump. As water evaporation took place, the dope rapidly cooled off to a temperature where evaporation became too slow to be effective, requiring frequent reheating of the dope. Water boiled off without incident while the dope was still fairly fluid, but as the dope thickened there was a tendency to form one large bubble rather than many small bubbles. At this point, if the pressure within the vacuum chamber was not monitored very closely, the bubble would burst violently. This often resulted in a loss of material, making it impossible to determine water concentration by monitoring evaporative weight loss. Crust formation continued to be a problem as the dope reached higher concentrations. The inability to monitor weight loss made it impossible to reproducibly concentrate dopes by this method, while crust formation resulted in inhomogeneous dopes. Clearly, this method was inadequate.

Use of a rotary evaporator allowed much better control over the evaporation process. This technique uses a round flask which is rotated in a warm water bath for even heating. The mouth of the flask is attached to a glass tube which runs into a water cooled condenser. Vacuum is supplied by a water aspirator pump, allowing better control over the pressure than that possible with a mechanical pump. This method was applied with much success, although it was still plagued by problems once the dope viscosity began to increase substantially. The large bubbles responsible for material loss in the first method could be avoided by very closely monitoring the pressure within the evaporator, however it was nearly impossible to avoid all of the bubbles all of the time. Rather than burst violently, the bubbles tended to move up the tube and into the condenser. Often a large amount of dope was pushed ahead of the bubble, and if not arrested in time, as much as half a batch could be lost due to a single bubble. Further concentration ultimately increased the viscosity to a point where large bubbles no longer formed, but crusting became an issue. Unlike the hot plate methods, the crust formed at the flask walls, making it possible to retrieve dope which was homogeneous. However, the crusted dopes were no longer homogeneous with respect to water content, and again it was impossible to determine water content based on weight loss. An additional drawback arose from the formation of bubbles too small to rise to the surface. These often led to spin line fractures or large voids which weakened the fibers.

The final concentration method was discovered accidentally during the first few trials using PEO as a binder. PEO was observed to behave in a similar fashion to PVP when concentrated in the rotary evaporator, except that the crust which formed in the flask could be redissolved in the dope that was still fluid. This behavior was further investigated by drying an entire batch of PEO-based dope in an oven at 65°C. It was found that the powders obtained from this drying procedure could be redissolved in water in a wide range of concentrations. Redissolution occurred in 18-30 hours, was observed to be unaffected by the molecular weight of the PEO, and the level of homogeneity was observed to be much greater than previously obtained. Defect causing bubbles were still observed, but in general were not as large or as plentiful as those observed in dopes prepared using rotary evaporation. Although the total amount of time to prepare a spinnable dope was about the same whether rotary evaporation or redissolution was used, redissolution did not require constant supervision as did rotary evaporation. A key aspect to this discovery was that a large amount of stock powder could be prepared and stored. Dopes of differing water concentrations could then be prepared from these powders, allowing reproducible spinnability experiments. All of the really serious developments in fiber processing took place after this discovery, and it could be said that the success of the entire project is due primarily to it.

2.1.4. Spinnability

Prior to the development of the redissolution technique of concentrating dopes, it was impossible to quantify spinnability as a function of water content. For this reason, no numbers can be given when discussing the spinnability of PVP dopes. Dopes prepared from PVP K-30 were found to be spinnable, but had poor wet strength. K-30 is mentioned in the patent literature as an effective spinning aid, so it is possible that the dopes prepared as part of this study simply were not concentrated enough. K-90 was found to be much more effective as a spinning aid, presumably due to its higher molecular weight. Solutions containing K-90/ceramic = 0.15 and an estimated 50 wt% water were found to be the most spinnable, although it was extremely difficult to concentrate dopes beyond this point using rotary evaporation.

The spinnability of PEO, on the other hand, could be investigated over a wide range of polymer and water concentrations. Experiments with single grades of PEO as binder revealed spinnability to increase with molecular weight. Fibers could be spun using WSR-205, however the spin line had very poor wet strength. WSR-303 was much more successful, and although of poor quality, fibers could be spun at concentrations as low as polymer/ceramic = 0.01. Higher quality fibers could be obtained using polymer/ceramic = 0.05, but phase pure YAG was difficult to achieve using WSR-303 as a binder. Since WSR-205 was found to be an effective colloidal stabilizer, experiments were performed using blends of WSR-205 and WSR-303 as the binder. These were discovered to not only stabilize the sols such that phase pure YAG developed in the fibers, but also were more spinnable than either was separately. Further experimentation showed that a 3:1 blend of WSR-205 and WSR-303 added to the sols in the proportion polymer/ceramic = 0.20 was the most effective at both producing phase pure YAG and at producing high quality fibers.

Spinnability as a function of water content was therefore investigated using sols produced with the 3:1 PEO blend. Fibers could be effectively spun at water concentrations between 30 and 40 wt%, with 35 wt% being optimum. Above 40 wt%, the dope was too fluid and tended to drip from the capillary. Below 30 wt% the dope was too viscous and led to disastrous spin line instabilities. It is possible that these highly viscous dopes would be spinnable with a different spinneret. For more on the influence of spinneret design on spinnability, see Section 2.2.2.

2.1.5. Summary of Final Sol-Gel Dope Preparation Method

Dope preparation begins with a yttria sol (Nyacol Colloidal Yttria, 14% in water), an alumina (boehmite) sol (Nyacol AL-20 Colloidal Alumina, 20% in water) and two grades of polyethylene oxide (Union Carbide WSR-205 and WSR-303). WSR-205 serves to stabilize the mixed sols while WSR-303 imparts spinnability. The PEO is received as a dry powder and must be dissolved in water prior to being added to the sols.

Dope preparation then proceeds as follows:

1). the ceramic yield of each sol is confirmed by calcination to 600°C
2). batch calculations are carried out using the following dry weight ratios; alumina/yttria = 0.753, WSR-205/total ceramic = 0.15, WSR-303/total ceramic = 0.05
3). the individual sols are then weighed out and WSR-205 solution is added to each, such that polymer/sol wt. is the same for each
4). the sol-polymer mixtures are allowed to stand for approximately 1 hour to allow homogenization and stabilization
5). the two sol+WSR-205 mixtures are mixed together and allowed to homogenize for 1 hour
6). WSR-303 is added to the sol+WSR-205 mixture and stirred vigorously
7). the mixture is poured into a long, flat dish and is dried at 65°C
8). the dried polymer+sol cake is lightly crushed (hard grinding may destroy the WSR-303 molecule) to form a stock of dry powder
9) a spinning dope is prepared by redissolving the powder in 35 wt% water

2.2. Fiber Spinning

When discussing the "spinnability" of a fluid, there is often ambiguity as to precisely what is meant. Ziabicki[7] defines a fluid to be spinnable if "it is capable of assuming large irreversible deformations when subjected to uniaxial stress, the measure of spinnability being the maximum attainable elongation." He goes on to point out that fluids such as honey and mineral oil are spinnable according to this definition, but are of course not fiber forming. In order for a fluid to be fiber forming, it must not only be spinnable according to the above definition, but the fluid stream must solidify in some manner so that the fiber is collectible. The form which "solidification" takes will naturally depend on the method of spinning. For melt spun fibers, this implies an actual solidification from the melt; for dry spun fibers, the evaporation of the solvent

which renders the dope fluid; and for wet spun fibers, a gellation or solvent removal process as a result of contact with the bath into which the fiber was spun.

Spinnability of developmental dry spinning dopes is often determined by hand spinning. This is usually accomplished by inserting a glass rod into the dope and removing it, pulling a fiber in the process. The degree of spinnability is then determined by the length of the fiber obtained. While in theory this may be a perfectly suitable method of determining spinnability, the current research has shown that in practice it can be quite a large step to scale a hand spinnable fluid up to a machine spinnable fluid. Although hand spinning served as a useful guide as to whether or not a particular dope would be spinnable, the dope ultimately had to be machine spinnable. Machine spinning was accomplished using small-scale fiber extrusion equipment supplied by Bradford University Research Limited (UK), shown schematically in Figure 2.1.

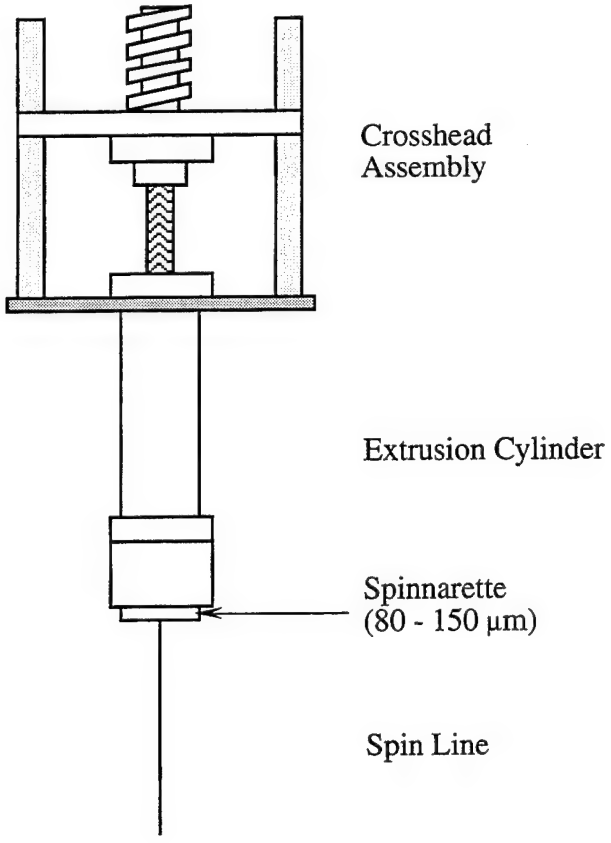

Figure 2.1: Schematic of Bradford Fiber Extrusion Machine

2.2.1. Hand Spinning vs. Bradford Fiber Extrusion Machine

Since the water content of PVP dopes was often indeterminate (see discussion in Section 2.1.3.), hand spinning was used as a guide to determine the point at which a dope was viscous enough to spin using the Bradford. The correlation between hand and machine spinnability was weak, thus repeatability was poor. However, hand spinning of PEO dopes was seen to be a necessary but hardly sufficient condition for machine spinnability. Dopes with as little as PEO/ceramic = 0.01 were hand spinnable at very high water concentrations, but only formed drops at the spinneret orifice during machine spinning. This emphasized the need for a systematic study of spinnability as a function of polymer loading and water content.

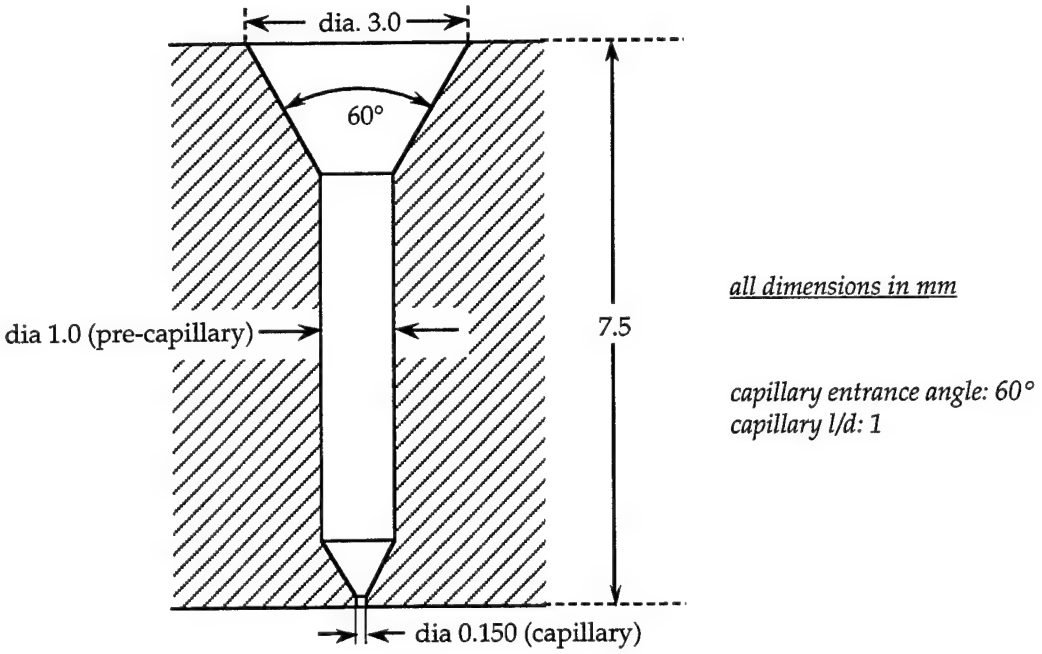

Figure 2.2: Typical Spinneret Geometry

2.2.2. Effects of Spinneret Size and Geometry on Spin Line

Once reproducible PEO-based dopes were available, it was possible to look at the quality of the spin line and the effect of spinneret geometry on spin line stability. All such experiments were performed using dopes prepared as described in Section 2.1.5. Figure 2.2 shows a spinneret typical of those used in this study. In all cases, spinnerets are identified by the diameter of the capillary, which is often considered to be the most important characteristic. However the aspect ratio, or length/diameter of the capillary is also very important, as are the diameter of the "pre-capillary" region and the entrance angle between the pre-capillary and capillary regions. Differences between spinnerets used in this study occurred mainly in the capillary and pre-capillary diameters. Three different spinnerets were used; an 80μm spinneret with a pre-capillary diameter of 2mm, a 150μm spinneret also with a pre-capillary diameter of 2mm, and a 150μm

spinneret with a 1mm pre-capillary. In all cases, l/d was 1 and the entrance angles were 60°.

A long spin line could be achieved using the 80μm spinneret, however the surface of the fibers thus obtained was extremely non-uniform, and almost kinked in places. The 150μm (2mm pre-capillary) spinneret also exhibited this behavior, although to a lesser degree. However, fibers spun using the 150μm (1mm pre-capillary) spinneret exhibited smooth surfaces with only occasional kinks.

The behavior observed in the first two cases resembles a situation described as melt fracture.[8] This form of spin line instability arises due to an elastic component in the viscosity of a fluid. When a fluid exhibiting an elastic component is deformed and released, it will partially "spring back" to its original shape, the amount of springback being determined by the length of time the fluid was held in the deformed shape. This situation is analogous to the time-dependent deformation of a solid, (strain-rate sensitivity) and may be modeled by a spring and a dashpot in series (Maxwell Model). As with strain-rate sensitivity, the degree of elasticity of a fluid may be characterized by a relaxation time - the longer the relaxation time, the more elastic the fluid.

As the fluid is forced through the spinneret, it must undergo deformations which are often very large. If, on exiting the spinneret, sufficient time for relaxation has not been allowed, the fluid will partially spring back. This behavior appears in its mildest form as die-swell. As it becomes more severe, the surface of the spin line is disturbed to a greater degree, ultimately resulting in spin line fracture. This problem is combated by changing the spinning conditions such that the residence time within the spinneret is relatively larger than the relaxation time of the fluid. This often may be accomplished by simply decreasing the spin line velocity. However, if this is not practical, changes in spinneret geometry must be made to either increase the residence time or decrease the amount of deformation the polymer experiences. Changes which will increase the residence time include a longer capillary (l/d increases), while those reducing the amount of deformation include a larger capillary diameter or a smaller pre-capillary diameter. This last condition may seem counter-intuitive, however, if large amounts of deformation are allowed to occur prior to the fluid entering the capillary, then much of the relaxation will have already taken place.

PEO is known to be a highly elastic fluid. Indeed, if a glass rod was inserted into one of the PEO/colloid dopes and quickly removed, the resulting fluid stream would fracture and *snap back*. Thus the extreme melt fracture observed from the 80μm spinneret was lessened by the larger capillary diameter and length of the 150μm (2mm pre-capillary) spinneret. The remaining surface instability was eliminated by the smaller pre-capillary of the 150μm (1mm pre-capillary) spinneret, although a significant amount of die swell was still present. This result was only recently discovered, and it is highly likely that a properly designed 80μm spinneret with $l/d > 1$ and a narrow pre-capillary would result in superior fibers to those produced as part of this study.

2.2.3. Fiber Takeup

Initially, attempts were made to spool the green fiber, however, this proved to be impractical. It was found that the spin line could not support any tension beyond that supplied by gravity, making spooling under tension impossible. This was unfortunate because it meant that the fiber diameter could not be controlled by drawing, and was therefore limited to the size of the spin line as it exited the spinneret. Observation of the spin line under tension revealed that failure always occurred at the spinneret face, presumably due to the low wet strength of the dope. It was possible to increase the wet strength of the dope by adding less water during redissolution therefore increasing the viscosity, however this only exacerbated the melt fracture condition described in Section 2.2.2. As it was observed that the green fibers could support tension, it is possible that a more viscous dope in combination with a spinneret which effectively suppresses melt fracture would permit control of fiber diameter through drawing. An additional spooling complication arose from the flexibility which the fibers maintained for several minutes after spinning. This flexibility allowed the fibers to be wound on a drum without breaking, however much of the flexibility had been lost by the time the drum was unwound. This resulted in curved fibers, which were difficult to straighten during firing.

Due to the problems associated with spooling, the spin line was allowed to fall from the spinneret without any tension beyond that provided by gravity. Fibers were collected by laying them down smoothly on a narrow strip of sheet steel, approximately one meter in length, passed underneath the spin line. When the end of the sheet was reached, the fiber was cut from the spin line and the direction of the sheet was reversed. This method resulted in reasonably straight green fibers which were easily inspected for large processing defects which had not caused spin line fracture. The length of the spin line was observed to be inversely related to its diameter; a spin line of approximately 2 meters could be maintained with the 80μm spinneret, while only 1 meter could be maintained with a 150μm spinneret. This was presumably a result of the greater weight of the larger spin line relative to the spin line cross section.

2.3. High Temperature Processing and Characterization of Fired Fibers.

Firing of the green fibers was a relatively straightforward procedure. The green fibers were insensitive to heating rate, and could be heated directly to the sintering temperature without intermediate dwells. There were no obvious problems with binder burnout from fibers spun with either PVP or PEO. However, if unconstrained during firing, fibers tended to curl. Curling had no bearing on the characterization of phase development, densification and grain growth, thus short lengths of fibers were fired unconstrained for these studies. However, mechanical testing and creep experiments demand straight fibers, necessitating the development of techniques for obtaining them. Figure 2.3 shows SEM micrographs of fracture and as fired surfaces of PEO-based fibers fired to 1500°C and 1700°C for one hour.

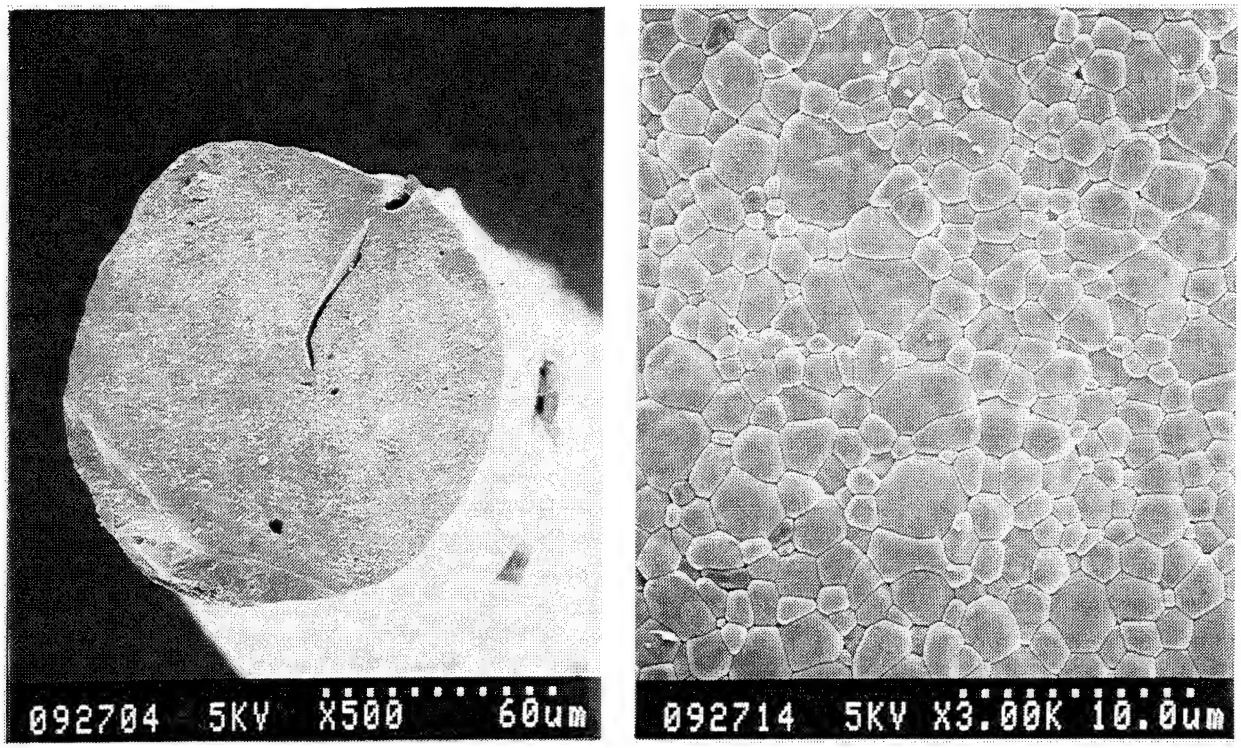

a)

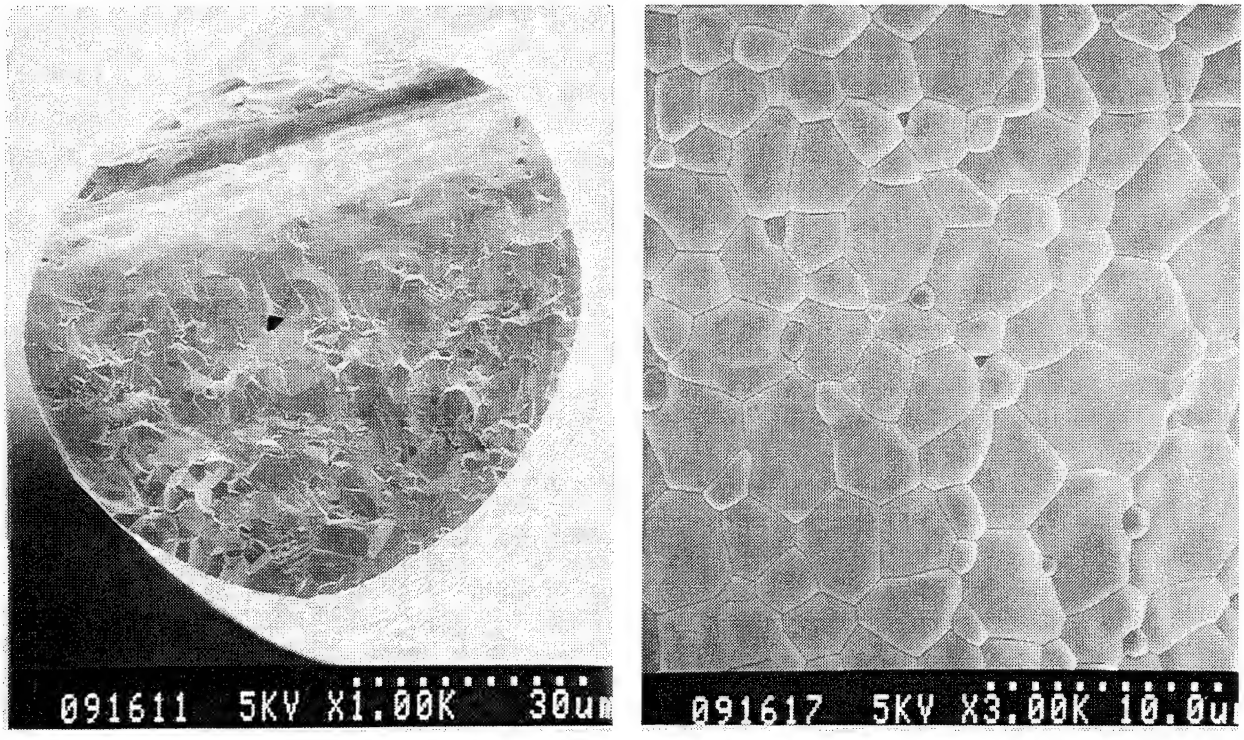

b)

Figure 2.3: PEO-based Fibers Fired to a) 1500°C and b) 1700°C

2.3.1. Densification and Grain Growth

Grain size measurements were made using Jeffries planimetric method. This method is performed by marking off an area of known size (a circle or rectangle, for example) on the micrograph of interest. A count is then made of the number of grains n_1 lying completely within this area, and the number of grains n_2 intersecting the perimeter of the test area. The total number of grains is then given by

$$N = n_1 + \frac{n_2}{2}$$

and the average area per grain is given by

$$\overline{A} = \frac{A_{test}}{N}$$

where A_{test} is the actual test area, adjusted for the magnification of the micrograph. The mean grain diameter is then given by

$$\overline{d} = \left(\overline{A}\right)^{1/2}$$

Grain size as a function of temperature was determined for temperatures between 1300°C and 1700°C for both PVP and PEO based fibers. Green fibers were placed in the hot zone of a Lindberg tube furnace which was already at temperature, and were held for period of one hour. SEM micrographs of the as-fired surfaces of these fibers were used in the study. The entire field of each micrograph was used as the area of interest. The grains were counted as described above, and A_{test} was determined by the dimensions of the micrograph normalized by the dimensions of the micron marker at the bottom of the photo.

Figure 2.4 plots grain size as a function of temperature. The grain size of the two different fibers was very close at low temperatures (1300°C), about 0.15μm. However, as the firing temperature increased, the grain sizes diverged. PEO-based fibers reached a maximum of 3.16μm while PVP-based fibers had a grain size of 2.18μm, a percent difference of 18%. The reason for this difference in grain size is not known, however it is most likely a result of subtle differences in dope homogeneity. Similar measurements for PEO-based fibers spun from dopes demonstrated by XRD to contain inhomogeneities exhibited grain sizes at 1700°C of around 1μm. It is tempting to conclude that the presence of second phases pinned the grain boundaries, restricting grain growth. However, there was no evidence that this was the case. It is possible that the presence of second phases influenced densification, which in turn influenced grain growth. However, there is not enough data at this time to attribute these differences to any one mechanism.

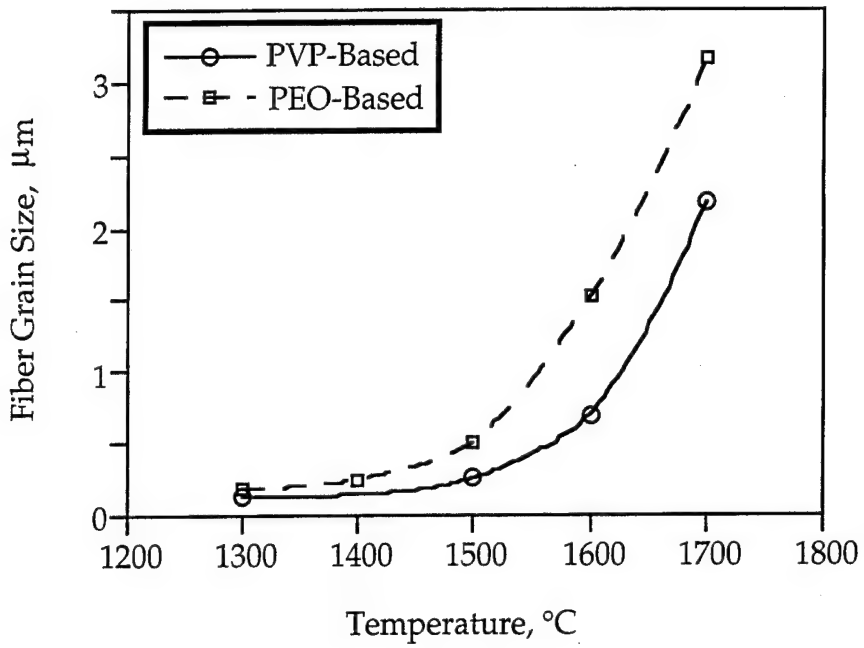

Figure 2.4: Grain Size as a Function of Temperature for PVP and PEO-Based Fibers

The as-fired surfaces of fibers were observed to be nearly fully dense by 1300°C, and completely dense by 1400°C. However, examination of fracture surfaces revealed significant amounts of porosity up to 1500°C. Only isolated pores were observed at 1600°C, and at 1700°C only processing related voids were present.

2.3.2. Phase Development

The phase development in the sol-gel fibers occurs gradually during heating, forming a sequence of intermediate phases. These can be followed through the X-ray diffraction powder patterns taken for gels heated for one hour at various temperatures. The dry gel is initially a diphasic mixture of yttria and poorly crystalline psuedoboehmite (AlOOH). Heating to 700°C dehydrates the psuedoboehmite to form an unreacted mixture of yttria and gamma-alumina. These two phases coexist without reaction to at least 900°C. Figure 2.5 shows diffraction patterns for fibers fired to temperatures between 1000°C and 1400°C and held for a period of one hour. At 1000°C, the yttria and alumina particles reacted to form $Y_4Al_2O_9$ monoclinic and $YAlO_3$ hexagonal. At 1100°C, a significant quantity of YAG had formed while the $Y_4Al_2O_9$ phase had almost disappeared and the $YAlO_3$ had transformed from the metastable hexagonal to the stable perovskite. At this point, $YAlO_3$ was referred to as YAP (yttrium aluminum perovskite). At 1200°C and 1300°C YAG is the predominant phase with only trace amounts of YAP. At 1400°C the fibers are single phase cubic YAG. It should be pointed out that excess alumina was rarely seen in the diffraction patterns, despite the fact that its presence was necessary to effect the complete transformation of the yttria rich $YAlO_3$ phase to YAG.

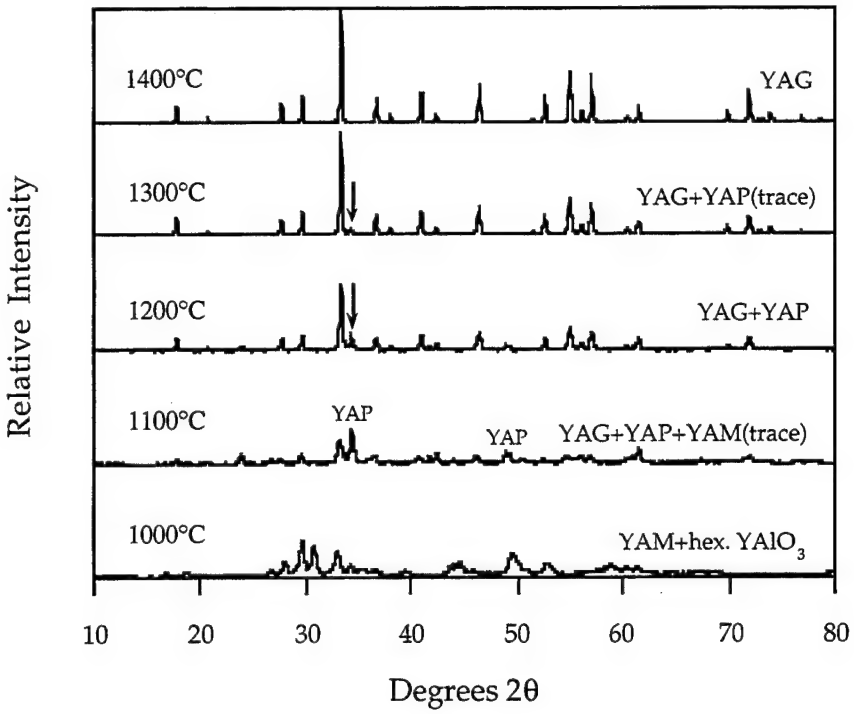

Figure 2.5: Phase Development of PEO-Based Fibers

2.3.3. Straightening Techniques

Fibers were observed to curl during firing if they were not constrained in some manner. Fracture surfaces of partially dense fibers often revealed areas of full density intermixed with areas of partial density. A difference in densification rate could lead to internal tensile stresses which would cause distortion during firing and the observed curling was attributed to this.

Firing straight fibers requires application of a tension to the fiber which is large enough to counteract the internal tension due to shrinkage during densification, but not so large as to cause structural damage. This would naturally occur during continuous fiber sintering, but we were not able to achieve this during this project. Instead, lengths of green fiber were fired under tension, by laying the fiber horizontally on a high purity alumina substrate and applying weights in the form of small blocks of high purity alumina refractory to each end of the fiber. As the fiber shrank during densification, it dragged the weight along with it, thus remaining straight. The amount of tension was determined by the mass of the constraining refractories, and this was adjusted by trial and error such that the fibers neither pulled free nor broke during shrinkage.

Fibers were fired in a Lindberg High Temperature tube furnace capable of 1700°C, and having a hot zone of approximately 24 cm. A sled was constructed using fibrous alumina refractory (Zircar SALI) as a base onto which a high purity polycrystalline alumina substrate was attached. Smaller pieces of the alumina refractory were then used as the weights. Temperature was monitored using an external Type B thermocouple. Fibers were fired to 1600°C and held for one to one and a half hours and allowed to furnace cool. Approximately 30% linear shrinkage could be expected during firing.

Although this technique successfully produced straight dense fibers, the longest fired lengths which could be practically obtained were approximately 13 cm. Since only two fibers could be fired simultaneously and each firing took roughly 5 hours to complete, producing any quantity of fibers was a very slow process. Furthermore, since the fibers were in frictional contact with the alumina substrate, there was always a possibility that surface defects could be introduced during the firing procedure.

2.4. Properties of Sol-gel YAG Fibers

Fiber specimens were too short to test using conventional tensile methods, so bending tests were used to characterize the mechanical properties of the YAG fibers. These consisted of bend strength determination at room temperature and creep tests using the Bend Stress Relaxation (BSR) method. Both techniques are derived from beam theory, involving a specimen which has been bent to a radius R. If the specimen is of uniform cross section along the axis, and pure bending may be assumed, then for an isotropic material, the stress $\sigma(z,R)$ at a point z from the neutral axis is given by

$$\sigma = \left(\frac{z}{R}\right)E \tag{1}$$

where E is the elastic modulus. If it can be assumed that the material behaves the same in compression as in tension, then the neutral axis and the centroidal axis coincide. In this case, the maximum stress can be obtained by substituting the fiber radius for z in the preceding equation. The value of the elastic modulus, E, was taken to be 284 GPa. The effect of pores in reducing the elastic modulus of the fibers was ignored.

2.4.1 Bend Strength Determination

A number of papers have been written on the subject of fiber strength determination by bending[9]. They all have equation 1 above in common, however, they differ in the technique of applying stress to the fibers and in the treatment of Weibull statistics, if performed at all. Several papers center around bending the fiber around drill bits of decreasing size until fracture occurs. The strength at failure is then taken to be the average of that obtained for the diameter at which failure occurred and the diameter previous to it. This is unsatisfactory because it not only requires repeated loading and unloading, it also does not give the stress at which fracture actually occurs.

Furthermore, the stressed volume decreases with drill bit diameter, an important consideration for attempting a Weibull statistics analysis.

In order to perform the test such that the stress was continuously increased in a constant volume of known size, an apparatus was constructed which allowed for the gradual decreasing of the bend radius, in such a way that the bend radius at the exact point of fracture was known to within the limits of human error. This technique also allowed for the stressed volume to be set prior to the test in such a way that it would remain constant throughout. Thus, the effect of stressed volume on bend strength could be determined.

The apparatus, shown in Figure 2.6 consisted of a plastic ruler which was attached to a wooden board by means of a vertical clamp. The fiber to be tested was attached to the outside of the ruler by means of orthodontal rubber bands. When the ruler was bent into a loop such that both ends contacted the clamp, a nearly perfect circle was obtained resulting in a state of nearly pure bending. The stressed volume of the fiber was then determined by the location of the rubber bands along the ruler, and the length could be read off directly. It was imperative that the fibers be placed on the outside bend of the ruler for several reasons. It was found that when attached to the inside, the fiber tended to pull away from the ruler and the actual bend stress was lower than that calculated by the radius of the bent ruler. Furthermore, the stress at the constraining point was higher than that calculated based on ruler diameter and failure always occurred at this location. By placing the fiber on the outside of the bend, not only was the bend stress known, but the point during the test when the fiber broke was quite apparent. The fracture could visibly be seen and often heard, thus further bending of the ruler could be avoided. After a short learning period, this method was highly effective, with each bend test taking only a few minutes of total elapsed time.

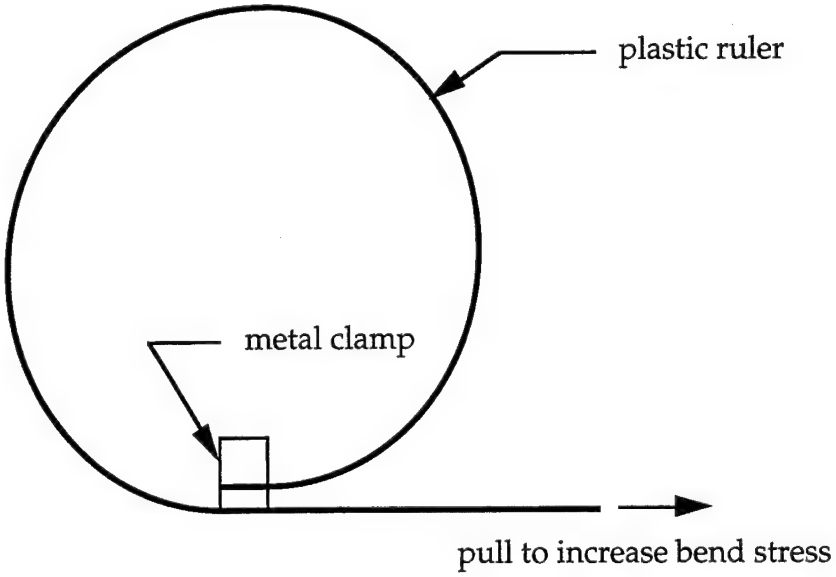

Figure 2.6: Bend Stress Testing Fixture

Bend tests were then performed by breaking a fiber of length, l_o and recording the radius at which fracture occurred. This resulted in at least two pieces, each of length $l<l_o$ which were fractured again. If it could be assured that no rotation took place between the initial fracture and the second fracture, (i.e. the tensile side from the first test remained the tensile side for the second test), then the stress at which the next fracture occurred would be greater than the initial fracture stress. However, it was rarely the case that no rotation took place, so it was not known *a priori* whether or not a fragment would be stronger than the original piece.

Once the test had been performed for a set of fibers, they were ranked according to stress at failure. The probability of failure below a certain stress level then became

$$F = \frac{n}{1+N} \tag{2}$$

where F = probability of failure at a stress level below σ_n
n = rank of stress σ_n
N = number of stress values recorded

These values were then used to determine the Weibull Modulus, as described below.

2.4.2 Weibull Modulus Development

A two-parameter form of the Weibull function

$$F = 1 - \exp\left[-\int_V \left(\frac{\sigma}{\sigma_0}\right)^m \frac{dV}{V_0}\right] \tag{3}$$

where dV = volume element
V = stressed volume
V_0 = reference volume
σ = stress on the volume element
σ_0 = scaling factor, often taken to be the stress at which $F(\sigma) = 0.632$
m = Weibull Modulus

is used to determine the form of the Weibull equation for the case of circular fibers of varying lengths tested in bending. Pure bending is assumed, so that the stress at a given distance from the neutral plane is constant along the length of the fiber. Therefore, the stress at any distance from the neutral plane can be found by

$$\sigma = \frac{Ez}{\rho} \tag{4}$$

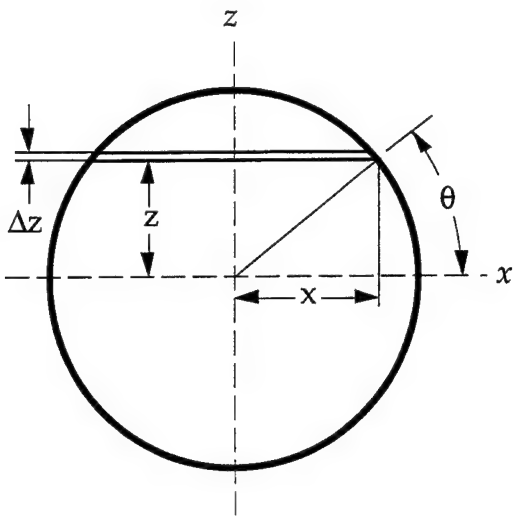

Figure 2.7: Schematic Fiber Cross-Section Showing Volume Element Used For Weibull Modulus Derivation

Figure 2.7 shows a schematic of the fiber cross-section. Bending occurs in the negative z-direction and the neutral plane intersects the x-axis. dV is taken to be a narrow strip running parallel to the neutral plane and only the tensile half of the fiber is considered. The volume element is then given by

$$dV = 2xl\,dz \tag{5}$$

However, x is a function of z. Cylindrical coordinates may be used to write Equations (4) and (5) in terms of a single variable, θ, thus

$$\sigma = \frac{Er\sin\theta}{\rho}$$

and

$$dV = 2lr^2\cos^2\theta\,d\theta.$$

Making the appropriate substitutions and rearranging, Equation (3) becomes

$$F = 1-\exp\left[-2\frac{lr^2}{V_0}\left(\frac{Er}{\sigma_0\rho}\right)^m\int_0^{\frac{\pi}{2}}\sin^m\theta\,\cos^2\theta\,d\theta\right] \tag{6}$$

The integral in Equation (6) cannot be solved symbolically for non-integer values of m, however a numerical solution exists. The value of the integral drops rapidly from 0.33 at m=1 to 0.076 at m=5, then drops gradually to 0.032 at m=10. For convenience, the integral is replaced with an arbitrary function of m, $f(m)$. The reference volume, V_0, can arbitrarily be chosen to be 1 cm^3, and therefore may be replaced by $l_0r_0^2$, where $l_0 = r_0 = 1$ cm. Then making the substitution

$$\sigma^* = \frac{Er}{\rho}$$

where σ^* is the apparent bend strength, Equation (6) becomes

$$F = 1 - \exp\left[-2\left(\frac{l}{l_0}\right)\left(\frac{r}{r_0}\right)^2\left(\frac{\sigma^*}{\sigma_0}\right)^m f(m)\right]$$

Replacing l/l_0 and r/r_0 with the dimensionless quantities l' and r', rearranging and taking the natural log of both sides twice yields

$$\ln\ln\left[\frac{1}{1-F}\right] = \ln\left[2(r')^2 f(m)\right] + \ln[l'] + m\ln\left[\frac{\sigma^*}{\sigma_0}\right]$$

The term $2(r')^2 f(m)$ is a constant (since r is known and $f(m)$ is a function of Weibull modulus only) and may be replaced by an arbitrary constant A. However, l' is not a constant, since fibers of different lengths were used for many of the tests. The term $\ln(l')$ can then be moved to the left hand side of the equation to yield

$$\ln\ln\left[\frac{1}{1-F}\right] - \ln[l'] = A + m\ln\left[\frac{\sigma^*}{\sigma_0}\right] \qquad (7)$$

which is the equation of a straight line with y-intercept A and slope m The data was then plotted as $\ln\ln[1/(1\text{-}F)]\text{-}\ln[l]$ vs $\ln[\sigma^*/\sigma_0]$. Although independently derived here, a similar approach to the length effect has been suggested before.[10]

2.4.3 Room Temperature Results

A typical fracture surface is shown in Figure 2.8. Fracture was initiated at defects on the surface, without exception. Very large internal defects could be present, but fracture was seen to always initiate at surface defects.

Table 2.1 lists the raw and reduced data. The average stress was found to be 522 MPa with a standard deviation of 186. This data is plotted in Figure 2.9 according to the equation above. The data is indeed linear, albeit with quite a bit of scatter ($r^2 = 0.8430$). The slope of this line and hence the Weibull modulus was found to be 3.5. Table 2.2 lists the Weibull moduli of several commercially available fibers. As can be seen, the experimental YAG fibers of this study compare quite favorably with other fibers in terms of Weibull modulus. The average strength of these fibers is not that high, but could be improved with improvements in processing.

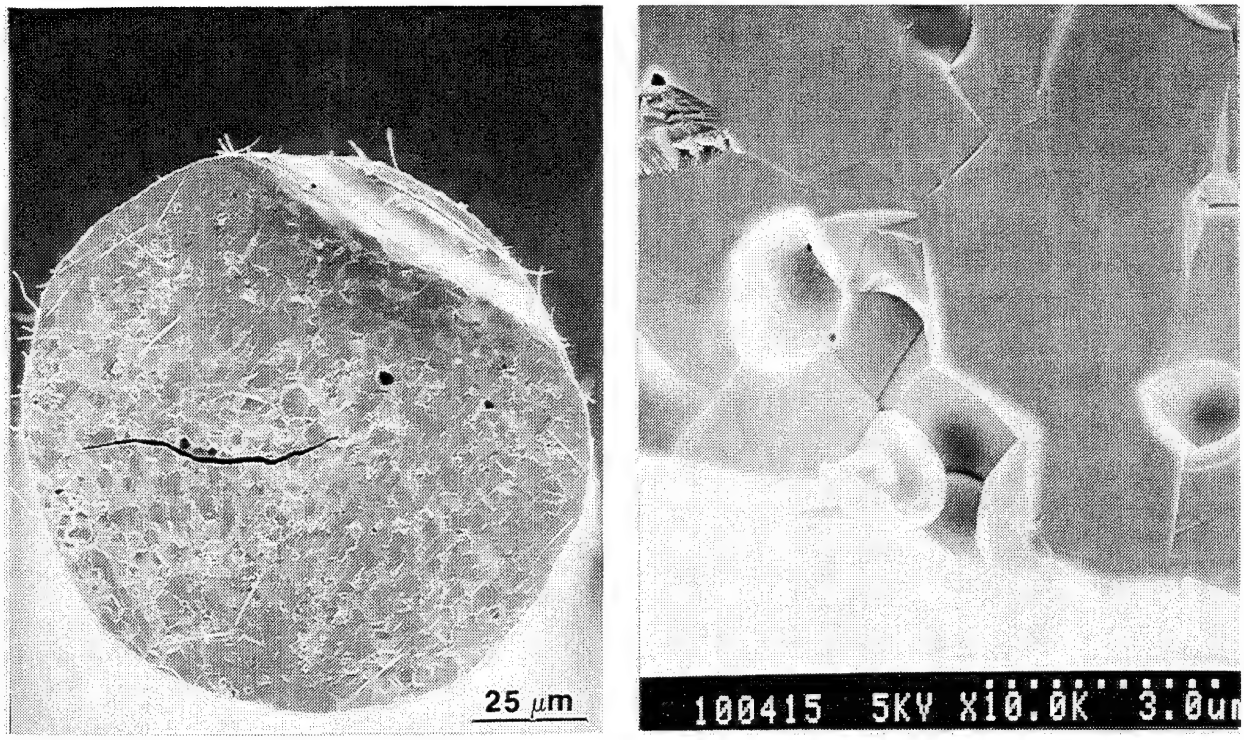

Figure 2.8: Typical Bend Stress Fracture Surface.
(note fracture initiated at fiber surface)

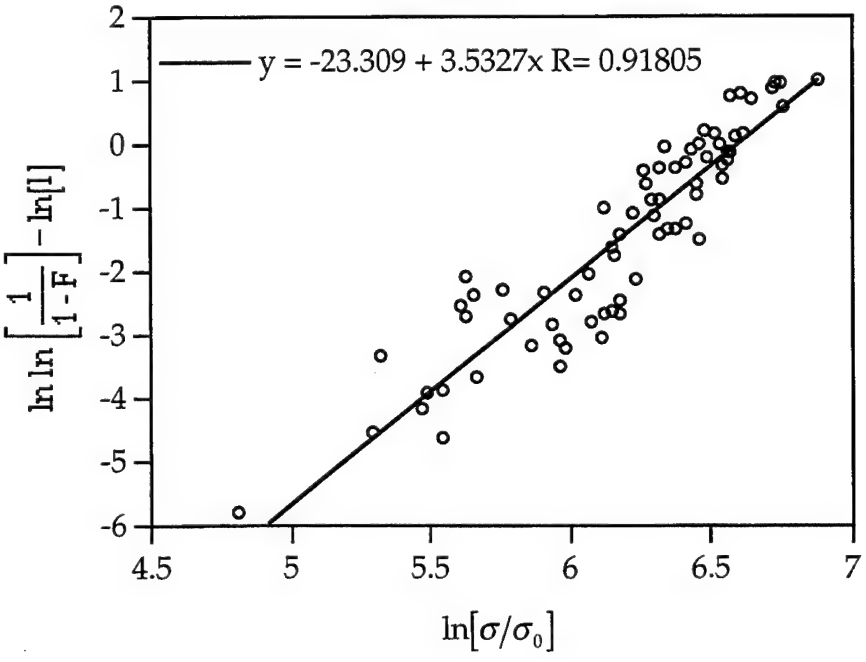

Figure 2.9: Weibull Plot of Cumulative Probability of Failure
with Increasing Bend Strength

Table 2.1: Bend Stress Data

Sample	Gage, cm	Radius, cm	Stress, MPa	rank
541	4.6	13.83	123	1
542	2.6	8.55	199	2
4512	1.2	8.30	205	3
456	3.6	7.17	237	4
441	3.6	6.99	243	5
451	9.0	6.66	255	6
452	5.0	6.64	256	7
458	1.5	6.24	272	8
553	2.0	6.12	277	9
4511	1.2	6.10	278	10
454	1.8	5.91	287	11
431	7.2	5.88	289	12
554	2.0	5.36	317	13
453	3.4	5.23	325	14
551	5.6	4.85	350	15
569	2.6	4.60	370	16
512	4.5	4.50	377	17
561	9.5	4.38	388	18
562	6.7	4.35	390	19
521	8.1	4.28	397	20
563	3.7	4.13	411	21
424	2.8	3.94	431	22
471	6.2	3.91	434	23
421	8.5	3.77	450	24
432	6.0	3.72	456	25
5613	1.2	3.71	458	26
531	6.6	3.62	469	27
566	2.5	3.62	469	28
552	3.0	3.60	472	29
511	6.2	3.52	482	30
465	2.3	3.52	482	31
461	8.4	3.51	484	32
567	1.8	3.35	508	33
422	5.4	3.33	510	34
459	1.0	3.25	522	35
543	1.3	3.21	528	36
514	1.7	3.15	539	37
564	2.3	3.11	547	38
5610	1.9	3.07	553	39
526	1.2	3.06	556	40
423	3.4	3.05	557	41
568	0.9	3.01	564	42

Table 2.1 (cont.): Bend Stress Data

Sample	Gage, cm	Radius, cm	Stress, MPa	rank
513	3.5	2.99	569	43
522	3.6	2.89	587	44
525	1.4	2.89	588	45
472	3.6	2.78	611	46
532	1.4	2.78	611	47
515	1.2	2.73	622	48
464	2.1	2.69	631	49
523	2.6	2.68	635	50
462	5.5	2.66	638	51
565	1.3	2.65	641	52
533	1.1	2.60	652	53
544	1.7	2.58	658	54
5611	1.2	2.53	672	55
456	1.5	2.47	687	56
475	2.2	2.45	693	57
463	2.8	2.44	696	58
442	2.2	2.41	705	59
433	2.0	2.40	708	60
5612	0.9	2.38	715	61
467	2.2	2.37	716	62
426	1.8	2.34	726	63
455	1.0	2.30	738	64
425	2.0	2.28	745	65
527	1.2	2.21	767	66
434	1.1	2.04	832	67
545	1.1	2.03	837	68
466	1.2	1.99	853	69
474	2.0	1.98	858	70
516	1.6	1.75	973	71
		average	522	
		st dev	186	

Table 2.2: Weibull Moduli of Experimental and Commercially Available Fibers

Fiber	Weibull modulus, m[11]
DuPont Fiber FP	6.5
Nippon Carbon Nicalon	3
Sumitomo Al_2O_3	4-6
3M experimental Al_2O_3	8.9
UM experimental YAG	3.5

Defects Affecting Strength: Although bend testing reveals only the effect of surface flaws on strength, there are other sources of weakness in the fibers. Large voids on the inside of the fiber are often noted, as well as large, central cracks which appear on the fiber axis. These defects stem from three different sources, all processing related. Large voids are related to the dope homogeneity. They can form either due to agglomerations formed within the sols or due to incompletely dissolved polymer.

Central cracks are related to drying shrinkage of the green fibers, and do not occur during the heat treating process. There are several observations which point to this conclusion. First, central cracks were often observed on green fibers which resembled the cracks observed in fired fibers. Furthermore, no additional cracking was noted on firing, whether the green fibers contained cracks of not. The appearance of cracks was also related to the age of the green fibers; fibers which were examined in the SEM several hours after spinning exhibited no cracks, while those examined several days after spinning did. Finally, central cracks were never observed in fibers spun from an 80 μm spinneret, but were often seen in those spun from the 150 μm spinneret. Thus it would appear that water evaporation was a time dependent process on the order of several days, and the strain imposed on a green fiber due to drying was sufficient to cause fracture in thick sections.

Surface defects could originate from any point between spinning and firing. There are several steps which involve handling the fibers, cracks could easily form as a result. The firing process itself (for straight fibers) requires the fiber to be in contact with an alumina substrate while moving across its surface. There is ample opportunity for defects to be introduced at this time. Clearly, what is needed to combat this rather detrimental source of defects is a method of producing green fibers which do not require as much handling, and which can be fired to a straight length without having to be in contact with a surface.

2.4.4 Bend Stress Relaxation Creep Tests

Creep of fibers usually involves very specialized creep stands and is extremely time intensive. To combat the problems associated with traditional techniques, Morscher and DiCarlo[12] at NASA Lewis devised a technique known as Bend Stress Relaxation (BSR). This method was used to evaluate the creep resistance of the experimentally developed fibers of this program. The results are compared to BSR results of commercially available fibers.

BSR tests consist of bending a fiber to a radius r such that a stress less than the fracture stress is imposed on the tensile edge of the fiber. The fiber is then placed in a furnace at the desired temperature and allowed to soak for a predetermined amount of time. On removal, the fiber is unloaded and allowed to return to zero strain. If no creep has taken place, it will spring back straight. However, if it has crept, there will be a residual amount of curvature in the fiber. This is measured and compared to the original radius of curvature via the stress relaxation ratio, defined as

$$m = 1 - \frac{r_o}{r_f}$$

where r_o = initial bend radius

r_f = bend radius after test

Thus, an m value of 1 indicates no creep whereas an m value of 0 indicates complete creep. This value has not been related to the steady state creep rate, however, Morscher has performed the test on a number of commercially available fibers, and so a large database exists with which to compare the results of developmental fibers.

There are two basic variations on the BSR test, both deriving from equation 1, in which a stress is imposed by bending. The first involves constraining the fiber to a constant radius, either by literally tying it in a knot, or by using a semi-circular fixture. In this case, the entire volume of fiber which is bent experiences the same stress. The second makes use of column buckling theory, in which the fiber is compressed axially such that it buckles. For the purposes of this test, it is assumed that the middle section is of relatively constant bending radius. This radius is measured, and the test performed as with the first method. On completion of the heat treating step, the fiber is removed from its constraint and the radius measured again. Graphical representation proceeds as it would with the constant radius test.

There are two main differences between these tests; constant radius vs. non-constant, and the size of the stressed volume. A much larger stressed volume may be obtained in the case of the constant radius test than in the case of the buckling test. A larger volume is desired because it makes the test statistically more significant. Also the types of radii required (in a practical sense) by the constant radius test make the radius measurement more accurate. However, the buckling test requires a lower stress level than the constant radius test, and thus is often more suitable for developmental fibers.

The creep tests performed in this study were done at NASA's Lewis Research Center in Cleveland, Ohio, using the buckling method. This was due to the high defect density of these fibers, making them too weak to withstand the stresses imposed by the constant radius test. Buckled fibers were treated for 1 hour at temperatures between 1100°C and 1400°C. The results of these tests are shown in Figure 2.10. Also plotted on this graph are the stress relaxation ratios (m) for several commercially available fibers for comparison. As can be seen from the stress relaxation ratios, the YAG fibers, although not that strong, were more creep resistant than every other fiber on the chart except for Saphikon's single crystal alumina. This result is in agreement with Corman's research which shows polycrystalline YAG to be highly creep resistant. Saphikon's fiber is c-axis oriented, so it should be more creep resistant, also in agreement with Corman.

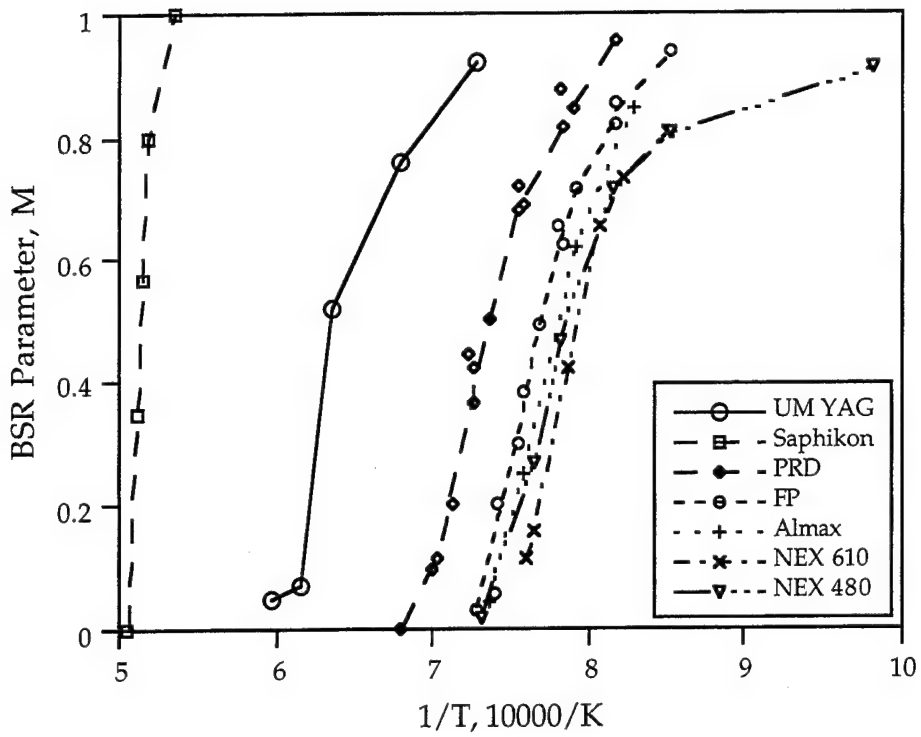

Figure 2.10: BSR Parameter of UM YAG and Several Commercially Available Fibers[9] (one hour at temperature)

2.5 Conclusions

It was found that phase pure YAG fibers could be prepared from aqueous colloidal sols using water soluble polymers as spinning aids. The type of polymer and its molecular weight were seen to influence phase development in the fibers. A blend of two different molecular weight grades of polyethylene oxide (PEO) was observed to be the best from the standpoint of spinnability and phase development. WSR-205 proved to be an effective colloidal stabilizer while WSR-303 imparted spinnability. Homogeneous spinning dopes could be prepared by first drying a mixture of sol+PEO and then redissolving the dried powders in a known quantity of distilled water.

Fibers could be continuously spun using the Bradford Small Scale Extrusion Device. The high degree of elasticity of the PEO molecule was seen to affect the quality of the spin line by enhancing melt fracture. The appearance of melt fracture was correlated to the geometry of the spinneret and spin line velocity. Melt fracture could be reduced by decreasing the rate at which deformation of the dope took place near the spinneret capillary. The spin line was seen to have insufficient strength for spooling and green

fibers conformed to the shape of the take-up drum. Straight green fibers could be collected on a flat surface passed beneath the spin line at a continuous velocity. Green fibers densified gradually over the range 1300°C-1600°C, but were fully dense at 1700°C. Transformation to YAG was complete by 1300°C-1400°C. Green fibers curled during firing if unconstrained, but could be constrained using fibrous alumina refractory weights. Large, central cracks were observed in fibers with diameters > 150 μm, their appearance being correlated with the amount of time between spinning and firing.

The bend strength of fibers was determined using a simple fixture that allowed continuous variation in the radius of bending. An average strength of 522 MPa was observed, although there were individual fibers which were much stronger. Bend strength was limited by surface flaws which were thought to be processing related. Due to the nature of the bend test, the bend strength was unaffected by internal flaws such as the observed central cracks. A modified Weibull treatment of the bend stress data revealed a Weibull modulus of 3.5. This value indicates a good deal of scatter in the strength of the fibers, although commercially available fibers also exhibit low Weibull moduli. Creep tests were performed using the Bend Stress Relaxation test developed at NASA's Lewis Research Center. Despite the low strength of the fibers, their resistance to creep was better than all commercially available polycrystalline alumina fibers. At a stress relaxation ratio of 0.5, the creep resistance of the YAG fibers was increased by 220°C over PRD 166 fiber and 275°C over Fiber FP alumina fibers.

Despite their superior creep resistance, the usefulness of the current fibers is limited by their low strengths. Attributed to an abundance of processing related defects, improvements in the processing would likely result in increased strengths. Despite the success of the "redissolution" technique of dope preparation, dope homogeneity could still be improved, possibly by the use of a low speed shear mixer. Further improvements in the green fibers could be realized by a thorough study of spinneret geometry. It is thought that a spinneret with substantially larger l/d ratios than those used in this study would result in superior fibers. It is further thought that the appearance of large central cracks could be avoided by the use of a spinneret with a smaller diameter capillary (< 100 μm). It is likely that additional surface flaws are introduced during the straightening procedure, during which the fibers are in frictional contact with an alumina substrate. Even in light of these difficulties, this technique for producing polycrystalline YAG fibers holds much promise. Dope preparation is relatively simple and the raw materials are inexpensive. All processing may be done in air and complex pyrolysis steps are unnecessary. Their superior creep resistance makes these fibers candidates for future high temperature applications.

3. YAG FIBERS FROM CARBOXYLATE PRECURSORS

Of the chemical approaches to ceramic materials (sol-gel and organometallic), the organometallic pre-ceramic processing route offers some advantages over sol-gel processing. Organometallic precursors rely on pre-formed bonding arrangements in the polymer, solvent selection, and polymer concentration for rheological control. Their rheological properties are controlled by hydrogen and electrostatic bonding, and mechanical crosslinking interactions rather than hydrolytically induced chemical (covalent) crosslinking. For this reason, organometallic precursor solutions are more suitable for fiber spinning and can generally be stored for long periods of time, without forming intractable gels.

Organometallic processing permits more effective atomic mixing of multimetallic systems than sol-gel processing. Atomic mixing in organometallic precursors relies on pre-formed organic bonding arrangements in the polymer. This permits more effective atomic mixing of the metal components than in sol-gel processing, as long as all the components dissolve completely in a suitable solvent.

Organometallic processing has some problems, such as: (1) effective removal of carbon containing ligands to minimize carbon impurities, and (2) the densification and accompanying volume changes that occur during formation of ceramic materials. Because the organic ligands must be removed, pre-ceramic polymers always have much lower densities than the target ceramic products. However, for thin films and fibers, the significant volume changes associated with organometallic processing are not a serious problem, because: (1) little or no mass transport and shrinkage occur in at least one dimension (in fibers, the axial dimension) which helps retain shape integrity, and (2) the diffusion distances for mass transport are very short in other directions (in fibers, the diametrical directions), so that gaseous byproducts are removed easily and the ceramic residues densified readily during pyrolysis.

These carboxylate precursors are based on isobutyrate systems previously developed for Y-Ba-Cu-O superconductor fibers[13]. and formate-acetate systems which have been used for alumina-based fibers[14]. Using these for YAG fibers presented considerable challenges. Both were developed into promising approaches for YAG fiber. Isobutyrates were emphasized during the first year of the program. Later we focused on the aqueous formate-acetates, which appeared more promising. At the end of the program, most activity was devoted to this system. In Section 3.1 we present first the formate acetate system. The results for isobutyrates are presented in Section 3.2.

3.1. YAG Fibers From Formate-Acetates

Yttrium and aluminum formate-acetates are prepared from aqueous solutions of aluminum formate and yttrium acetate. Our approach differs from the conventional formate-acetate approach[15], in that we do not use boric acid-stabilization of the aluminum acetate solutions. In this way we avoid contaminating the final ceramic fiber

with B_2O_3, but it is much more difficult to obtain stable aqueous solutions at high concentration.

3.1.1 Formate-acetate Dope Formulations

The formate and acetate solutions can be made spinnable in several ways. With the addition of lactic acid, the solutions can be concentrated to yield a viscous polymeric solution suitable for hand drawing fibers as fine as 10 microns. However, continuous fibers could not be extruded from the lactic acid containing solutions because of their low elasticity and wet strength, causing spin line fractures under modest drawing conditions. Polyvinylpyrrolidone (PVP) is used as spinning aids. The PVP increases the elasticity of the spin dope, improves drawing behavior, and increases green strength of the dry fibers.

The formoacetate precursor formulation was under constant development. The favored formulation for spinnable formoacetate solutions at the end of the program used 7 wt% polyvinylpyrrolidone (PVP), using either grade K90, K-120, or K-30. To prepare this dope, the Y-acetate and Al-formate are dissolved in a large excess of water and mixed with the ethylene glycol. This mixture is heated to evaporate essentially all of the water. The formoacetate concentrate is mixed with an aqueous solution of PVP. This is further concentrated by evaporation of the water. The spinnable concentrate composition is:

Y-acetate wt%	Al-formate wt%	Ethylene glycol wt%	PVP wt%	Diethylene glycol wt%
37.8	32.1	11.7	7	0.7

A second dope, leading to a pinning phase, was needed for bicomponent spinning experiments. The yttrium-rich YAM phase was a candidate, so a formate-acetate YAM precursor was produced. A high concentration YAM precursor solution was obtained at a ligand ratio of 0.234 moles acetate/mole formate. At other ratios, precipitation occurs. Fibers were spun successfully with precursor solution with the following composition: Y-acetate, 8.72 gm; Al-formate, 2.05 gm; formic acid 14 gm; water 80 gm, ethylene glycol 1.8 gm, PVP-K30 grade of polyvinylpyrrolidone 0.9 gm. A clear spinnable solution is obtained after concentration in a rotary evaporator. Thin fibers, 10μm in diameter, could be prepared and cured to 230°C. This mixture produced nearly single phase YAM at 1400°C.

Towards the end of the program, an all-formate process was evaluated for a YAG precursor from Y-formate and Al-formate. This required the synthesis of yttrium formate from yttrium carbonate. Yttrium carbonate tri-hydrate (2.4 mmole, 1g) was reacted with formic acid (14.4 mmole, 0.68 g) to make yttrium formate, via:

$$Y_2(CO_3)\cdot 3H_2O + 6HO_2CH \rightarrow 2Y(O_2CH)_3 + 6H_2O + 3CO_2$$

Yttrium carbonate tri-hydrate was mixed with 100 ml of water. The yttrium carbonate tri-hydrate is insoluble in water, what when the formic acid was added, the solution bubbled as carbon dioxide escaped and the mixture became a clear solution. The correct stoichiometric amount of aluminum formate (4 mmole) was added, and mixed with 0.25 g of lactic acid. After the solvent was removed on a heating plate, a spinnable solution was obtained.

3.1.2 Fiber Spinning

The formate-acetate dope is readily spinnable in air. Green fibers with diameters between 10-20 μm were continuously spun on the Bradford and collected on a spool. Figure 3.1 shows a typical as-spun formate-acetate fiber.

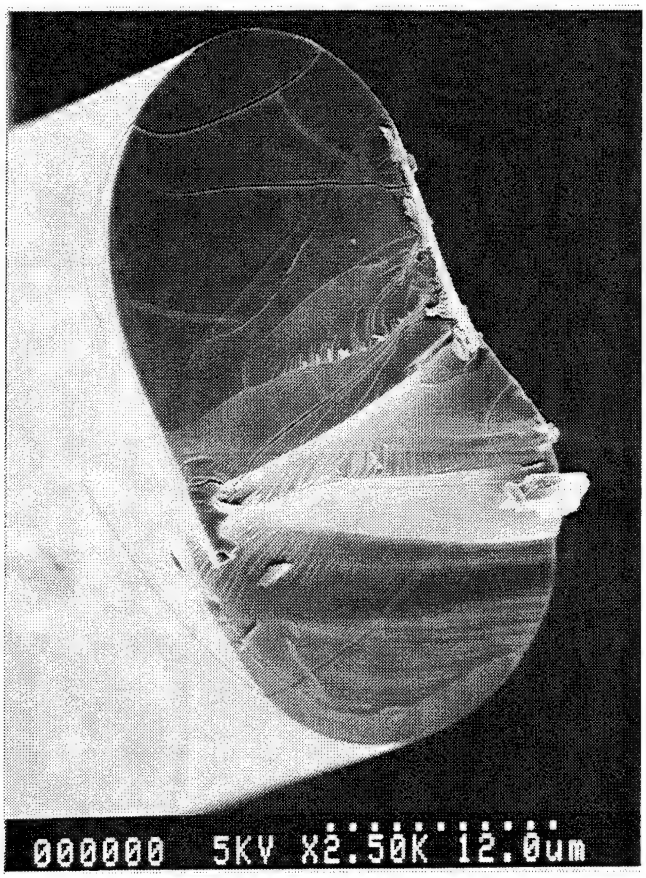

Figure 3.1: As-spun Formate-Acetate Fiber

3.1.3 Pyrolysis and Sintering

The as-spun formate-acetate fibers have a nominal composition $(Y_3Al_5(OH)_y(OOCH)_{15-y}(OOCCH)_{9-y}\text{-}nH_2O$. Phase diagrams[16], suggest 2-3 waters of

hydration should be present per metal atom, so n is about 16-24. The degree of hydrolysis, y, is not known. Figure 3.2 shows its TGA-DSC behavior at a heating rate of 1°C/min. in air. The waters of hydration are lost during the endothermic event near 120°C, with a corresponding weight loss of 25-30%. The oxidative decomposition of the acetate and formate occurs in three exothermic events between 300 - 470°C, associated with an additional 25-30% weight loss. The solid residue of these reactions should be yttrium oxycarbonate and γ-Al_2O_3[17,18]. The small endotherm and 3% weight loss above 800°C is attributed to decomposition of the oxycarbonate to oxide. Weight loss is complete above 850°C. The mass yield of YAG is about 35%, while the inferred volume yield from dry Y-Al formate-acetate to YAG is about 10%.

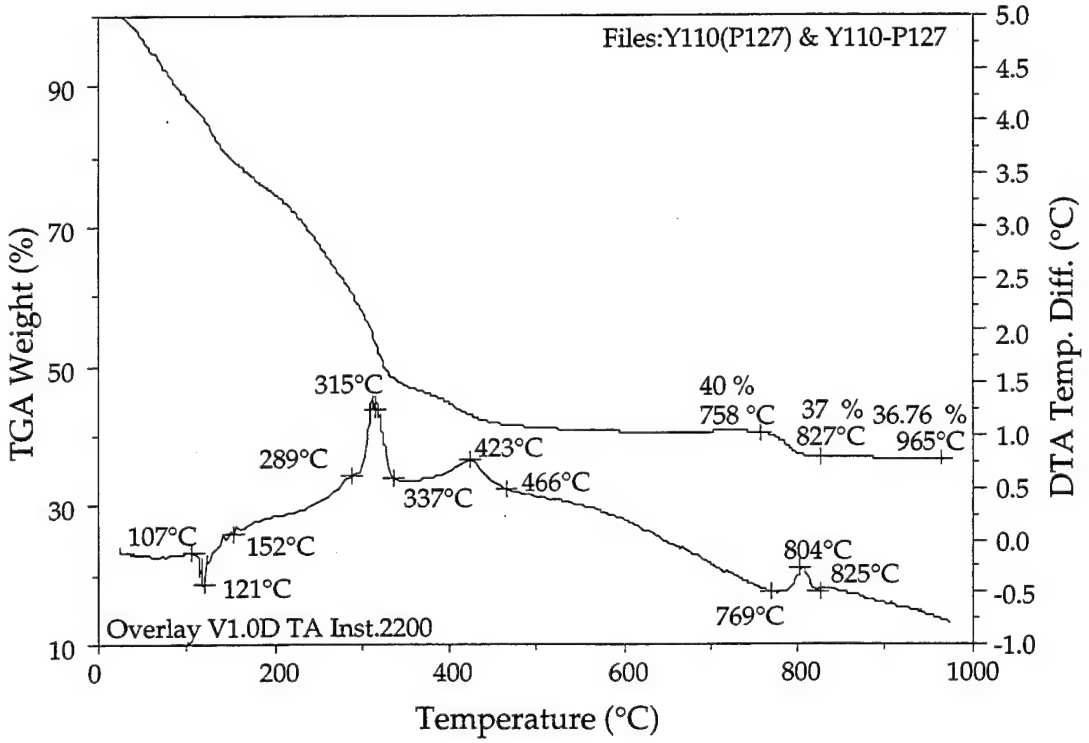

Figure 3.2: TGA and DTA of Formate-Acetate Precursor Mixed in YAG Stoichiometry (heated at 1°C/minute)

Rapid release of the waters of hydration can cause the formate-acetate fibers to bloat around 100°C, creating a foamy solid. The appearance of the foam suggests that the hydrated Y-Al formate-acetate melts to a viscous hydrated liquid before losing the hydration water, similar to the decomposition behavior of yttrium formate hydrate. Fiber with a diameter around 20 microns do not bloat, probably because the since water can diffuse out more easily. Figure 3.3 a) shows a 6-micron diameter fiber heated to 1000°C without cracking. At this point it is not yet densified, but consists as an intimate mixture of 100-200 nm YAG grains with fine interparticle porosity.

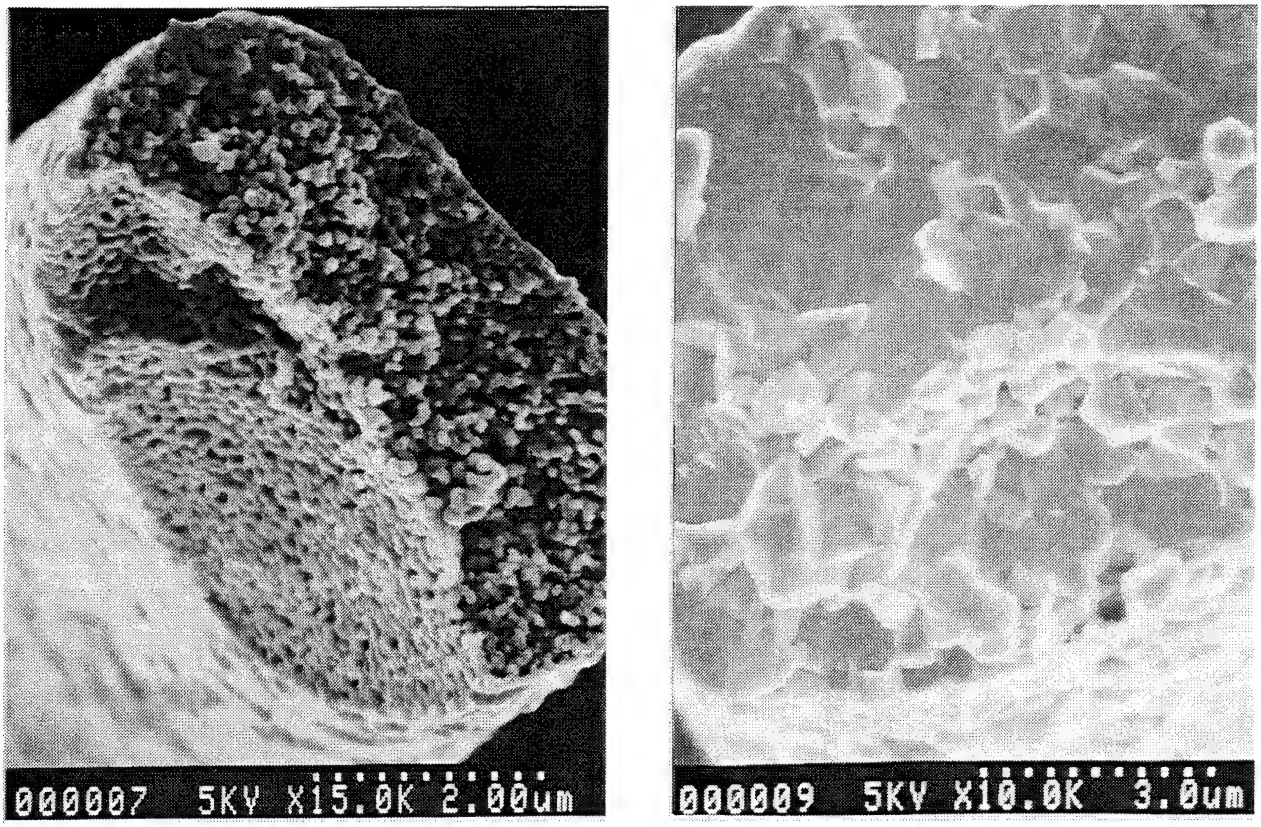

a) b)

Figure 3.3: Formate-Acetate Derived YAG Fibers a) Heated to 1000°C Without Cracking and b) sintered at 1500°C

Like the isobutyrates, the formate-acetate fibers sinter to good density upon rapid heating, but remain porous if heated very slowly. Figure 3.3 b) also shows the microstructure of a formate-acetate derived YAG fiber after heating at 20°C/hr to 1500°C, with a 1-hour hold. The YAG has sintered to about high density, with a 500-1500 nm grain size.

Slow heating produces porous fibers. Figure 3.4 is an example of a porous fibers with a hollow core. This structure was frequently observed after inappropriate pyrolysis and sintering. Much effort was devoted to studying pyrolysis, to identify effective processing windows and to discover the origin of the pathological densification of hollow core fibers. Unfortunately, no clear pattern could be found. A second curious phenomenon was the effect of fiber diameter. Formate-acetate fibers with green diameters larger than about 20 μm would also develop the porous "unsinterable" microstructure, often with a central void.

We had shown that this problem could be overcome by rapid heating, leading to dense, sound YAG. We were surprised when the sintering problem re-appeared, even with fast heating. This led to a careful study of pyrolysis. Fibers were pyrolyzed at

rates varying from 5°C/min. to 25°C/min. to 1400°C. All rates other than 10°C/min. produced the unsinterable microstructure. At 10°C/minute, the YAG sintered well, producing an essentially pore-free fiber. Apparently the processing window is narrow, with poor results with slower or faster heating. The reason for this curious phenomenon is not known.

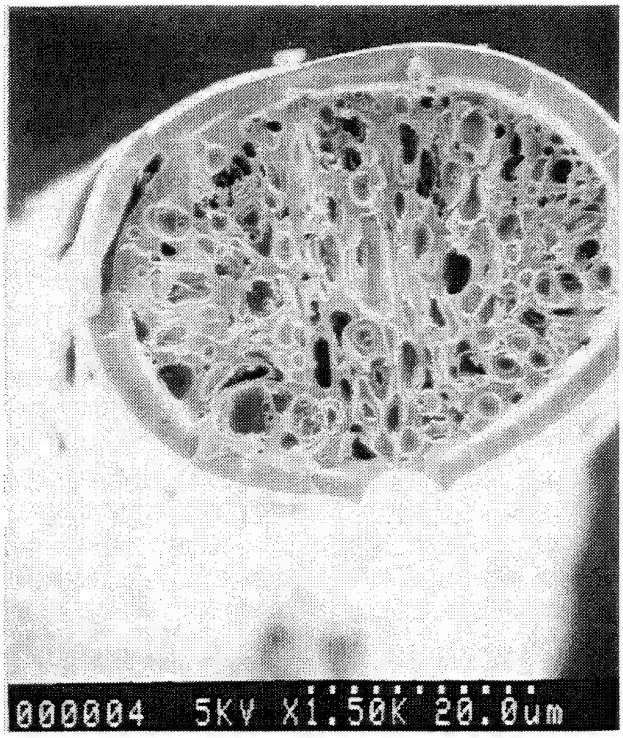

Figure 3.4: Formate-Acetate Derived YAG Fiber Exhibiting Hollow Core on Firing

We undertook a systematic experimental matrix to define the correct heat treatment. The heat treatment was divided into four steps, each associated with major events during pyrolysis, as indicated by thermal analysis. These events are: i) endothermic dehydration, which we prefer to do at 80°C to avoid bloating; ii) carboxylate decomposition, which occurs exothermically between 200 and 600°C; iii) yttrium oxycarbonate decomposition and YAG crystallization, around 800°C; and iv) densification around 1500°C.

The following heat treatment parameters were varied:
1) dehydration ramp, 2) temperature, and 3) dwell;
4) decomposition ramp, 5) temperature, and 6) dwell;
7) crystallization ramp, 8) temperature, and 9) dwell;
10) densification ramp, 11) temperature, and 12) dwell;
and 13) atmosphere (wet air or dry air) in various steps.

About 25 experiments were conducted with systematic variations of these parameters, followed by SEM examination of the microstructure of the YAG fibers at

several stages of the process. The study identified two heat treatment sequences leading to dense sintered fibers. These were:

Treatment A	Treatment B
1) 2°C/min., 2) 80°C, and 3) 4 hr; 4) 2°C/min., 5) 275°C, and 6) 4 hr; 7) no crystall. step, 8) ---, 9) --; 10) 20°C/min., 11) 1500°,12) 2 hr; and 13) dry air in all steps.	1) 2°C/min., 2) 80°C, and 3) 4 hr; 4) no decomp. step, 5) ---, 6) ---; 7) 5°C/min., 8) 800°, and 9) 2 hr; 10) 20°/min., 11) 1400°, 12) 4 hr; and 13) moist air steps 1-9, dry air in steps 10-12.

Other treatments resulted in poor densification or the central void problem.

3.2. YAG Fibers from Isobutyrates

We have previously shown that metal carboxylates, especially isobutyrates permit facile processing of organometallic precursor fibers.[12] Furthermore, they are easily synthesized. Thus, we chose to explore the utility of 3:5 mixtures of Y and Al isobutyrates as precursors to polycrystalline YAG.

In this section, we describe: (1) the syntheses of the Al and Y isobutyrates, $Al(O_2CCH(CH_3)_2)_3$ and $Y(O_2CCH(CH_3)_2)_3$; (2) the reactivity patterns of the individual carboxylates, and of 3:5 (Y:Al) stoichiometric mixtures of these compounds during their pyrolytic transformation to phase pure Y_2O_3, Al_2O_3 and YAG respectively, and (3) preliminary studies on fiber processing.

3.2.1 Experimental Procedures

Isobutyric acid (99%) was purchased from Pfaltz and Bauer Inc. Isobutyric anhydride (97%) was purchased from Aldrich Chemical Company. Toluene, THF, (from Mallinckrodt Co.) and MeCN (J. T. Baker) were distilled from the appropriate drying agents under N_2 and stored under N_2 prior to use. Al powder (< 8 Mesh, from Allied Chemical and Dye Co.), and Y chips (Morton Thiokol, Inc.) were used as received. All reactions were run under N_2 in standard schlenkware.[19]

Synthesis of aluminum isobutyrate, $Al(O_2CCH(CH_3)_2)_3$: (1) A mixture of 2.4 g (88 mmol) Al powder, 70.0 ml (755 mmol, about 2.9 equivalents) isobutyric acid, 2.0 ml (12 mmol) isobutyric anhydride, and 200 ml toluene (as solvent) were mixed with a catalytic amount of $HgCl_2$ (0.1 g, 0.4 mmol) to a 500 ml schlenk flask. The mixture was then heated to reflux with stirring. The color of the reaction solution changed to dark gray as Al powder was consumed. (2) The solution was allowed to react for 4 days, then cooled and filtered through a medium size frit. The recovered solid was collected

and recycled. (3) The filtrate was filtered again through celite to give a clear solution. Solvent was removed by vacuum evaporation at 120°C to give an off-white solid $Al(O_2CCH(CH_3)_2)_3$ (11.4 g, 46% yield). (4) The recovered mixture of toluene and other liquid residuals (e.g. anhydride) was then mixed with the recovered solid filtered from the synthesis reaction. The mixture was then heated and stirred at reflux to dissolve a further portion of the recovered solid. An additional 2.35 g of product was obtained, by repeating steps (2) and (3) to give a net yield of 55%. The product is THF soluble; however, if the filtered THF solution is exposed to air, it rapidly becomes cloudy, indicating moisture sensitivity.

Syntheses of yttrium isobutyrate $Y(O_2CCH(CH_3)_2)_3$: Yttrium metal shavings (12.7 g, 143 mmol) were placed in a schlenk flask with 60 ml (650 mmol) isobutyric acid (1.5 equivalents), 2.0 ml (12 mmol) isobutyric anhydride, 200 ml THF and 0.10 g (0.4 mmol) $HgCl_2$ as catalyst. The mixture was refluxed under N_2 until no further H_2 evolution (24 h) was observed. The hot solution was filtered through celite and allowed to cool. The $Y(O_2CCH(CH_3)_2)_3$ product precipitated out of solution on addition of 200 ml dry MeCN. After washing 3 times with 100 ml MeCN, the product was vacuum dried at 120°C, for 2 h. The white solid product was ground into a powder with alumina pestle and mortar. The yield was 34 g (97 mmol, 70% of theory).

YAG precursor solution: A 3:5 stoichiometric precursor solution, $3Y(O_2CCH(CH_3)_2)_3$: $5Al(O_2CCH(CH_3)_2)_3$, was formulated by dissolving 7.54 g (21.5 mmol, 43 weight percent) Y isobutyrate and 10.0 g (38.5 mmol, 57 wt. percent) Al isobutyrate in 100 ml of THF. Isobutyric acid (0.2 ml) was added to aid dissolution. The yttrium isobutyrate used was 10% less than the formula ratio because 10% of aluminum isobutyrate was insoluble in the THF. The solution was filtered to remove the small amount of insoluble matter. The solvent volume was then reduced by vacuum evaporation until the viscosity was suitable for hand drawing fibers (final volume 30 ml).

Characterization methods: Density measurements were used to establish the theoretical volume changes expected during conversion of precursor to ceramic. The Al-isobutyrate, Y-isobutyrate and YAG precursor, were ground in the glove-box and the powders were removed and rapidly pressed into 1.28 cm diameter cylindrical pellets with an applied pressure of 1.5×10^4 Pa for 15 sec. The carboxylate complexes deform plastically. The resulting pellet is assumed to be nearly 100% dense. Calipers were used to measure the dimensions of compacted pellets to determine the densities.

Ground samples of Y and Al isobutyrates and YAG precursor were put into separate alumina boats, 1 g per experiment, and heated in dry air at 5°C/min. to 300, 500, 700, 800, 900, 1000 or 1400°C for 2 h in a Thermolyne Type 6000 Furnace (Barnstead Thermolyne Co., Dubuque, IA).

TGA studies were conducted using a Hi-Res TGA 2950 Thermogravimetric Analyzer, TA Instruments Thermal Analyst 2200 (TA Instruments, Inc., New Castle,

DE). Samples (10-30 mg) were placed in a Pt pan and heated in dry air at 5°C/min. to 1000°C with an air flow rate of 60 cc/min.

DTA experiments were conducted on a DSC 2910 Differential Scanning Calorimeter (TA Instruments, Inc., New Castle, DE). Samples (10-20 mg) were loaded in a Pt crucible and heated at 5°C/min. to 1500°C in dry air at a flow rate of 50 cc/min. The DTA reference was alpha-alumina (Aluminum Co. of America, Pittsburgh, PA).

Diffuse reflectance infrared Fourier transform spectroscopy (DRIFTS) studies were performed using a Mattson Galaxy Series FTIR-3000 (Mattson Instruments, Inc., Madison, WI). Samples were prepared in a glove-box (N_2 environment) using crystalline KBr. The KBr was optical grade random cuttings commercially available from International Crystal Laboratories (Garfield, NJ). The KBr was ground in a mortar and pestle, and 600 mg weighed out. Then 3.6 mg sample (0.6 wt. percent of KBr) was weighed out and transferred to a mortar and pestle, and ground. Approximately the same amount of KBr was added and ground to thoroughly mix. The remaining KBr was added in successive portions to approximately double the total amount of material in the mortar. Each addition was followed by thorough grinding. Finally, the sample was transferred to the IR sample holder and quickly placed in the IR sample chamber, which was kept under constant N_2 purge. The chamber was flushed with N_2 for at least 10 min. before data collection. A minimum of 64 scans were collected for each sample at a resolution of 2 cm^{-1}. IR peak positions were identified using a standard peak searching program.

The nuclear magnetic resonance (NMR) spectra were obtained on a Brüker Aspect 3000, AM-360 NMR (Brüker Instruments, Inc., Manning Park, Billerica, MA) spectrometer operated at 360 (^1H), or 90.6 (^{13}C) MHz using 30 degree pulse widths and relaxation delays of 1.0 (^1H) and 0.5 (^{13}C) sec. Y-isobutyrate and Al-isobutyrate samples were dissolved in DMSO-d_6 (Aldrich Chemical Company Inc., Milwaukee, WI) under Ar. All signals are referenced to TMS (Aldrich Chemical Company Inc., Milwaukee, WI).

The pyrolytic transformation of the precursor to crystalline YAG, as a function of processing temperature, was followed by XRD, using a Rigaku Rotating Anode Goniometer (Regaku Denki Co. Ltd., Tokyo, Japan). Samples (40-80 mg) were prepared in a manner identical to that used for the DRIFTS samples. The powders were then loaded in x-ray sample holders (glass plates) for data collection. The working voltage and current were 40 kV and 100 mA respectively. Cu Kα (l = 1.54 Å) radiation with a Ni filter was used. Scans were continuous from 5 - 80 degrees 2θ with a step scan of 10° 2θ per minute and increments of 0.05° 2θ. The peak positions and the relative intensities of the sample patterns were identified by comparing with standard JCPDS files.

Fiber drawing and extrusion: Precursor fibers were both hand drawn and extruded. For hand drawn fibers, a small spatula was dipped into the viscous solution (under N_2) and withdrawn. The resulting fibers were suspended from a wooden framework (10 cm x

10 cm) and left to dry in the N_2 environment. In this case, green fibers about 30 μm in dia. and 200 mm in length were obtained. The extrusion spinneret diameter was 140 μm. Ordinarily, 2 ml precursor solution was loaded into the chamber of the extruder. The piston was pushed down by gas pressure to extrude the fibers. Gas pressures of about 300 psi were used to control the rate of extrusion. Because of self-drawing, thicker or thinner fibers could be collected at different distances below the spinneret. The thinnest, continuous fibers obtained were about 70 μm dia. and were collected across a square dowel framework 10 cm below the spinneret. Because of the rapid rate of solvent evaporation and Al-isobutyrate moisture sensitivity, continuous fibers with the dias. < 60 μm could not be obtained even when the fibers were drawn in tension.

3.2.2 Results and Discussion

In this section, we will discuss: (1) synthesis of Al and Y isobutyrates, (2) characterization of these isobutyrates, (3) bulk pyrolysis decomposition patterns for both the individual precursors and the YAG precursor, (4) studies on fiber processing.

3.2.2.1 Synthesis of $Al(O_2CCHMe_2)_3$: Aluminum isobutyrate was synthesized according to reaction (1):

$$Al + 3Me_2CHCO_2H \xrightarrow{\text{THF/toluene/trace } HgCl_2\text{/reflux in } N} 1.5H_2 + Al(O_2CCHMe_2)_3 \qquad (1)$$

To limit moisture degradation of the Al-isobutyrate, e.g. via reaction (2), isobutyric anhydride was used to remove any adventitious H_2O in the reaction environment. Aluminum hydroxide scale at the Al powder surface appears to cause formation of $Al(OH)(O_2CCHMe_2)_2$ rather than $Al(O_2CCHMe_2)_3$, as confirmed by direct reaction of $Al(OH)_3$ with isobutyric acid and anhydride (3). The detail will be discussed in DRIFTS section.

$$Al(O_2CCHMe_2)_3 + H_2O \longrightarrow Me_2CHCO_2H + Al(OH)(O_2CCHMe_2)_2 \qquad (2)$$

$$Al(OH)_3 + 2(Me_2CHCO)_2O \longrightarrow 2Me_2CHCOOH + Al(OH)(O_2CCHMe_2)_2 \qquad (3)$$

3.2.2.2 Characterization of $Al(O_2CCHMe_2)_3$:

Thermal analyses: Based on our previous studies of isobutyrates, the Al isobutyrate was expected to decompose primarily to the oxide at about 400°C:[6]

$$Al(O_2CCHMe_2)_3 \xrightarrow{400°C} Al_2O_3 + Al_2(CO_3)_3(\text{traces}) + \text{gaseous byproducts} \qquad (4)$$

The TGA profile for Al isobutyrate decomposition (Figure 3.5) shows two weight loss processes, first from room temperature to 90°C, and second from 180 to 360°C, with a final 19% ceramic yield. The first process arises because of moisture sensitivity, as determined by a TGA experiments run at room temperature in air. A sample of Al

isobutyrate was found to lose 16% of its original weight in 6 h, simply as a result of its brief exposure to air during the time it was weighed into the TGA sample pan. The weight loss is explained by the evaporation of isobutyric acid formed by hydrolysis of Al isobutyrate (reaction 2). The second weight loss arises because of oxidative decomposition of the organic ligands primarily to CO_2 and H_2O. The corresponding DTA (Figure 3.6) exhibits an exotherm at 270 to 360°C.

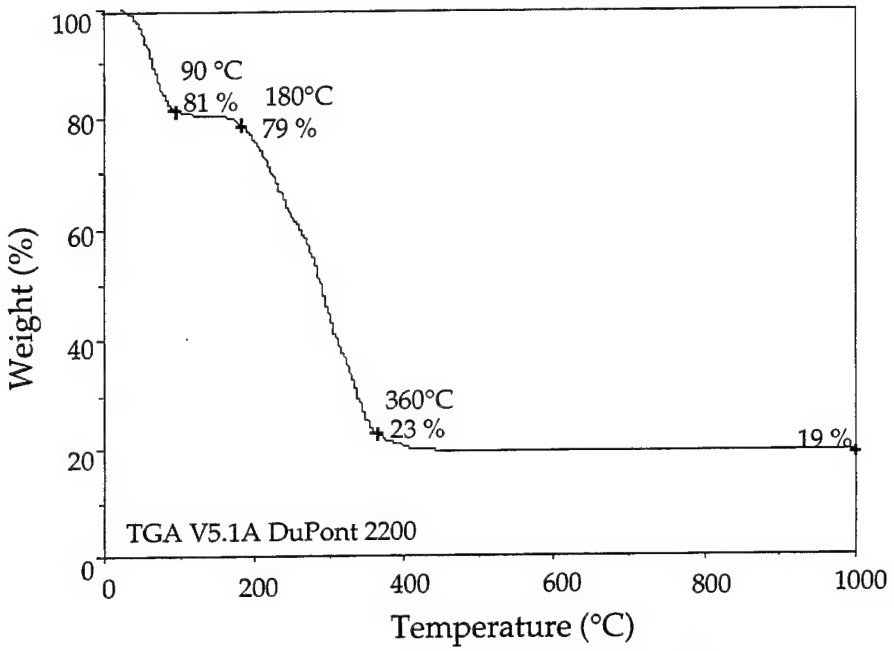

Figure 3.5: TGA of Aluminum-Isobutyrate Precursor

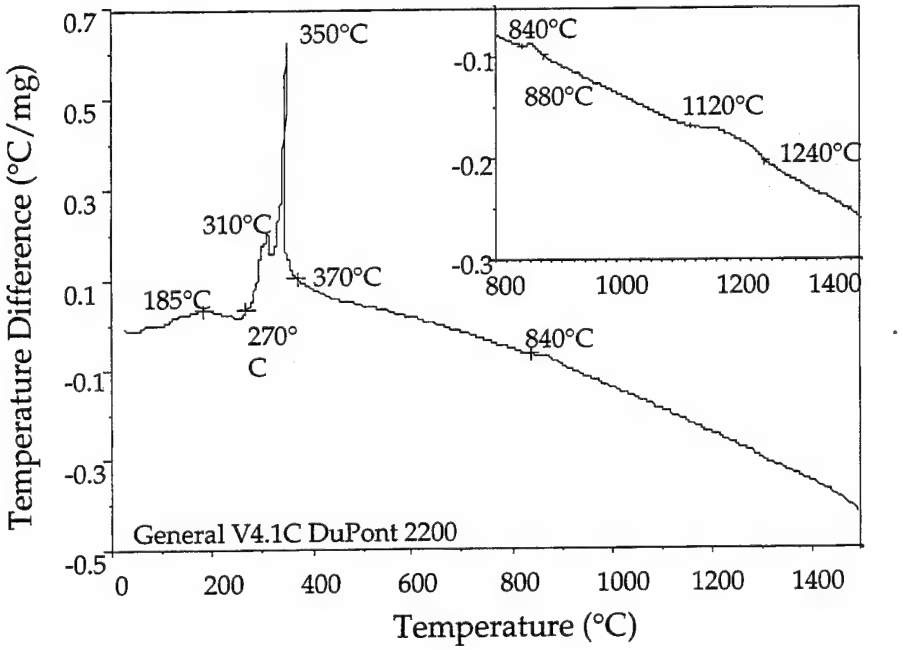

Figure 3.6: DTA of Aluminum Isobutyrate Precursor

The ceramic yield is slightly higher than calculated (18%) based on the formula, $Al(O_2CCHMe_2)_3$, and reaction (4). The presence of an OH band in the DRIFT spectrum (see DRIFTS section), suggests that the slightly higher ceramic yield is due to some $Al(OH)(O_2CCH(CH_3)_2)_2$ produced either via reaction (2), or by reaction of surface $Al(OH)_3$, with isobutyric anhydride, reaction (3). The ceramic yield for $Al(OH)(O_2CCH(CH_3)_2)_2$ is 23%. Thus, the ceramic yield for our precursor can be anticipated to be slightly greater than expected for $Al(O_2CCH(CH_3)_2)_3$ alone.

The Figure 3.6 DTA does not provide details about high temperature phase transformations because the sample size above 400°C is too small to compare with the reference, Al_2O_3 (at 400°C, the sample is 4 mg, 20 wt % of its initial weight). Optimal DTA analyses require that the sample weight approximate that of the reference to optimize observed temperature differences. For this reason, a precursor sample was first pyrolyzed to 500°C for 2 h. Then the same quantity of sample and reference (usually 20 mg each) were used to run the DTA (5°C/min./air) to 1400°C to obtain the inset in Figure 3.6. The inset shows two phase transformations, at 840-880°C and at 1120-1240°C. The XRD data for Al isobutyrate (Figure 3.7) suggests that the 840-880°C exotherm corresponds to amorphous alumina transforming to d-alumina, while the 1120-1240°C exotherm corresponds to crystallization of alpha-alumina.

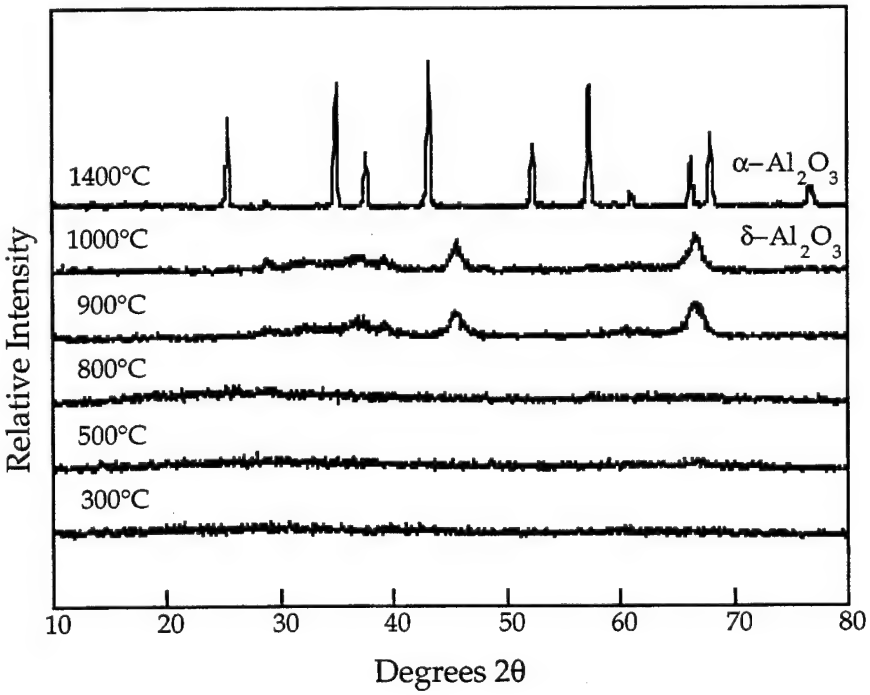

Figure 3.7: XRD Patterns of Aluminum Isobutyrates Fired to Various Temperatures

X-ray powder diffraction (XRD) patterns: Figure 3.7, the XRD data for Al-isobutyrate heated to selected temperatures for 2 h in air (heating rate 5°C/min.), shows that the material remains amorphous from 300°C to 800°C. At 900°C, the powder pattern reveals low intensity, broad peaks indicative of partial crystallization of d-alumina. Following heating to 1000°C, the peaks sharpen and grow in intensity as crystallization continues. At 1100°C, as supported by the DTA data alpha-alumina begins to crystallize. However, a well-defined alpha-alumina XRD pattern is obtained only following heating to 1400°C.

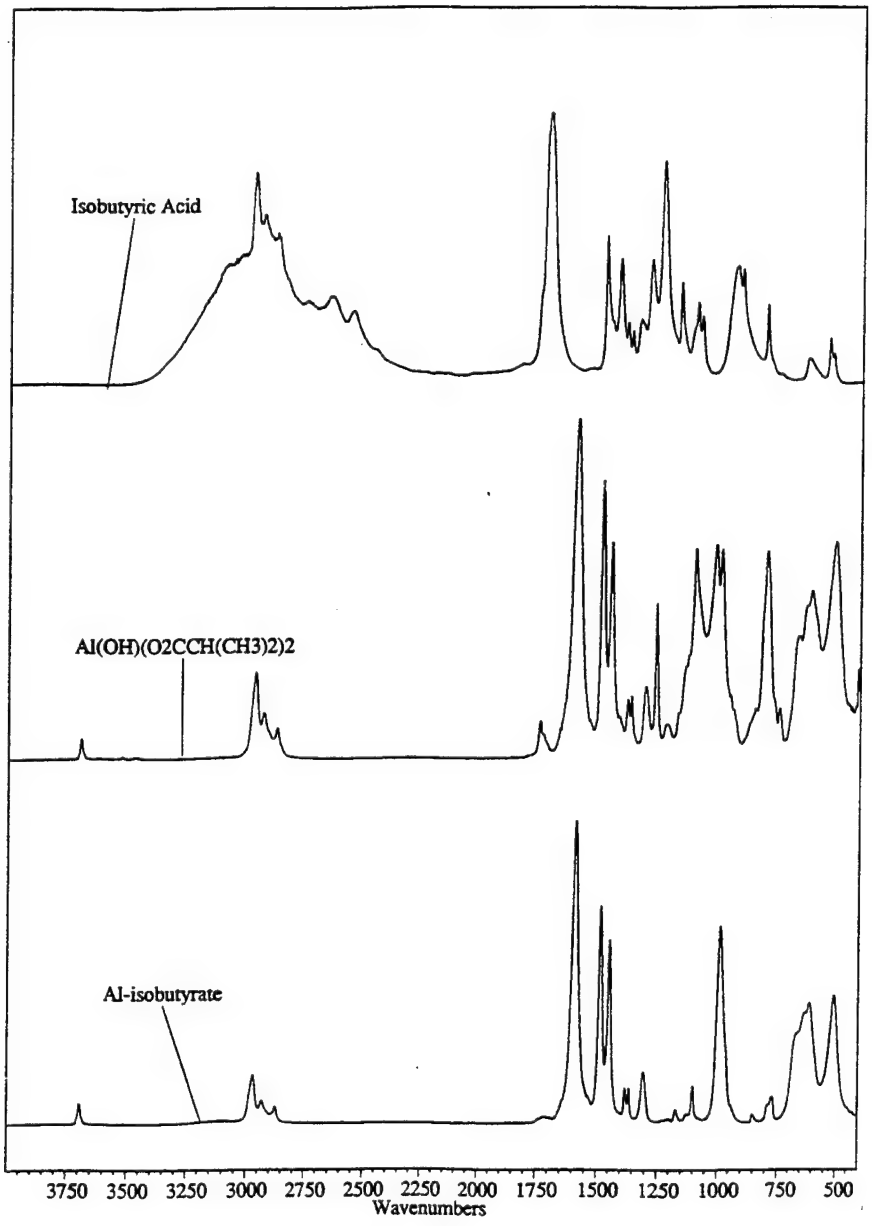

Figure 3.8: DRIFTS Spectra for Aluminum Isobutyrates

Diffuse Reflectance IR Fourier Transform Spectroscopy (DRIFTS): Detailed IR analyses of various metal isobutyrate precursors, including Y isobutyrate, are reported in the superconductor papers. The Al isobutyrate spectra shown in Figure 3.8 and the data recorded in Table I were analyzed by comparison with published data.[20] The antisymmetric nC=O band (1706 cm^{-1}) of free isobutyric acid (Figure 3.8a) is shifted to lower wave numbers (1540-1590 cm^{-1}) on complexation with Al (Figures 3.8b and c), as expected for organic acid salts. The peak (Figure 3.8b and c) at 3670 cm^{-1} (nO-H) indicates the presence of $Al(OH)(O_2CCH(CH_3)_2)_2$ as corroborated by comparison with an authentic sample (Figure 3.8b) prepared by reaction of $Al(OH)_3$ with isobutyric acid and isobutyric anhydride, reaction (3). Although efforts were made to limit sample exposure to humidity, it is likely that samples adsorb traces of moisture during transfer from the glove-box to the IR sample chamber, resulting in some hydrolysis. Note that DRIFTS preferentially shows the sample surface which is exposed most during sample transfer.

Table 3.1: DRIFTS Data for Y and Al Isobutyrates*
(a. Antisymmetric stretch, b. Symmetric stretch)

Isobutyrates	νC-H	νCOO[a]	νCOO[b]
$Al(O_2CCHMe_2)_3$	2978, 2945, 2887	1588	1477, 1448
$Y(O_2CCHMe_2)_3$	2974, 2934, 2875	1540	1477, 1430
Me_2CHCO_2H	2979, 2940, 2882	1706	1477, 1416

The small peak at 1706 cm^{-1} in the DRIFTS of aluminum isobutyrates (Figure 3.8b and c) corresponds to the nC=O of trace amounts of free isobutyric acid. This contaminant does not influence the final ceramic product, as all the organic ligands and Al-OH groups are eliminated during pyrolysis. The Al carboxylates were also characterized by NMR (see below).

DRIFT spectra of Al-isobutyrate heated to selected temperatures at 5°C/min. for 2 h complement the XRD and TGA/DTA studies providing a view of the transformations at the atomic scale. The spectra show that on heating to 300°C, the peaks at 3670 cm^{-1} (nO-H), 2887, 2945 and 2978 cm^{-1} (nC-H), and at 1588, 1477 and 1448 cm^{-1} (nC=O) are eliminated. The resulting spectra are indicative of an amorphous, inorganic material.

In the 300°C spectrum, new peaks at 1465 and 1585 cm^{-1} indicate formation of carbonate, CO_3^{2-}, e.g. $Al_2(CO_3)_3$. The absence of a powder diffraction pattern in the XRD suggests that the carbonate is amorphous, of insufficient quantity to register (less than 2%) or that the crystallite sizes are small. Because the peak intensities are relatively weak, it is likely that very little carbonate forms.

* The data reported are specific, strong absorption bands for the anhydrous, acid free complexes and is not meant to be comprehensive. Accuracy is $\pm$ 2.5 cm^{-1} (from reference 19).

By 500°C, the carbonate bands disappear indicating $Al_2(CO_3)_3$ decomposition.[21] The only other absorption bands of note are those attributable to surface Al-OH groups (nO-H, 3200-3400 cm^{-1}) which are present in the spectra up to 600°C. These groups disappear on heating to 700°C. No corresponding weight change occurs in the TGA, which supports the assignment as surface species. The DRIFT spectra change very little above 700°C, indicating that atomic level reorganization is complete by this temperature.

Nuclear magnetic resonance studies: ^1H and ^{13}C solution NMR were used to establish the solution structures of the metal carboxylates. Comparison with literature values confirmed the anticipated resonances and molecular structures.

3.2.2.3 Synthesis of $Y(O_2CCHMe_2)_3$:

Yttrium isobutyrate was synthesized according to reaction (5) using published procedures:

$$Y + 3Me_2CHCO_2H \xrightarrow{\text{trace } HgCl_2 \text{ /THF reflux}} 1.5H_2 + Y(O_2CCHMe_2)_3 \quad (5)$$

3.2.2.4 Characterization of $Y(O_2CCHMe_2)_3$:

Thermal analyses: Under the conditions studied here Y isobutyrate decomposes thermally as shown below:

$$Y(O_2CR)_3 \xrightarrow{400°C} Y_2O_3 + Y_2(CO_3)_3(\text{minor}) + \text{gases}(CO_2 + H_2O + \text{propene} + \text{other}) \quad (6)$$

The TGA profile (Figure 3.9) is rather straightforward with a single mass loss occurring between 260 and 360°C, corresponding to oxidative decomposition of the complex. The DTA (Figure 3.10) also exhibits a single major event in the same temperature range. Above 360°C, the TGA indicates a slow, minor mass loss corresponding to loss of residual carbon as CO_3^{2-} (see DRIFTS studies). The ceramic yield for Y-isobutyrate is 32%, exactly as calculated for $Y(O_2CCH(CH_3)_2)_3$, given reaction (6).

DRIFTS: Figure 3.11 displays DRIFTS spectra for Y isobutyrate heated to selected temperatures (5°C/min. in dry air) for 2 h. As with the Al isobutyrate studies, the DRIFTS studies provide a view of the transformations at the atomic scale. The spectrum of Y isobutyrate is very similar to that of the Al complex, showing nC-H bands at 2875, 2934 and 2974 cm^{-1}, and nC=O bands at 1430, 1477 and 1540 cm^{-1}. Likewise, Y-isobutyrate decomposes on heating to 300°C with concomitant formation of new peaks at 1404 and 1520 cm^{-1}, indicative of carbonate species, e.g. $Y_2(CO_3)_3$. The carbonate band intensities are greater relative to those observed in the Al isobutyrate decomposition. Furthermore, these peaks remain when samples are heated to temperatures of at least 800°C; although the intensities diminish as expected based on the slow but continuous weight loss observed in the TGA from 500 to 800°C.

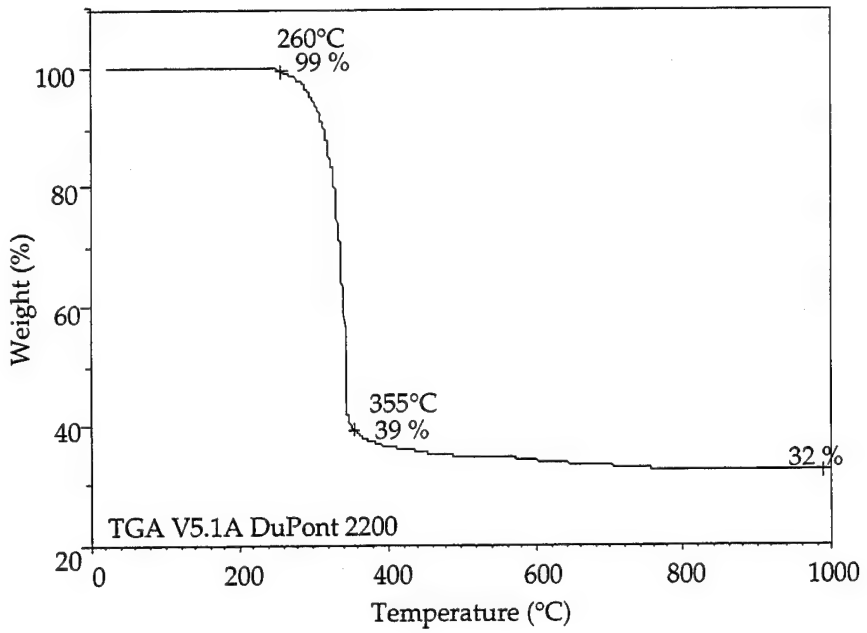

Figure 3.9: TGA of Yttrium Isobutyrate

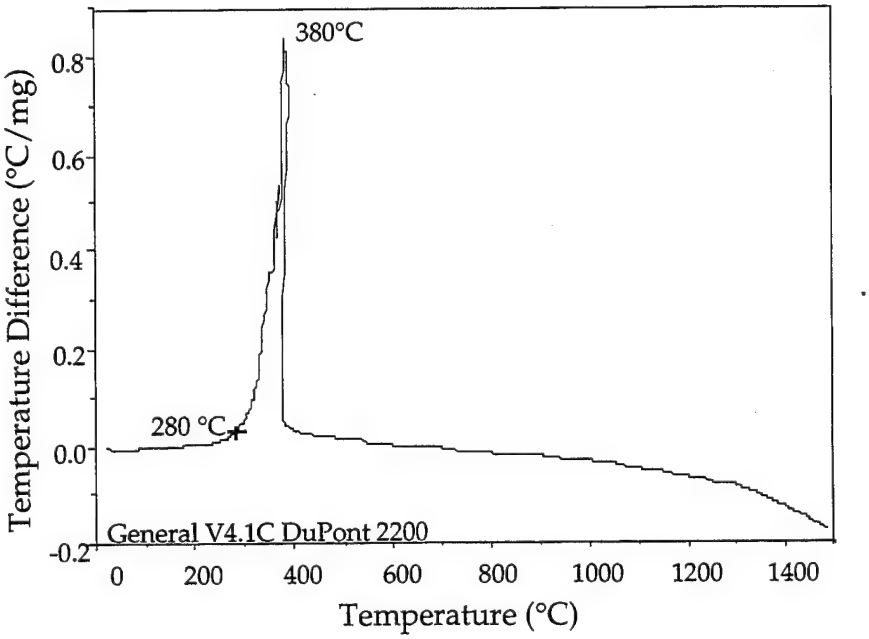

Figure 3.10: DTA of Yttrium Isobutyrate

As in the Al isobutyrate decomposition, Y-OH peaks appear in the region 3100-3600 cm^{-1}, coincident with the formation of the carbonate species. These peaks also persist to 800°C, but diminish in intensity as the pyrolysis temperature increases. In both instances, it is assumed that hydroxyl peaks are lost through a surface diffusion process that eventually leads to evolution of water.

A sharp peak appears at 560 cm^{-1} in the 500°C DRIFTS sample and grows in intensity at higher temperatures. This peak corresponds to nY-O and indicates formation of localized crystallinity, as discussed in the XRD section. In contrast, the XRD powder patterns, show no evidence for formation of crystalline carbonate species.

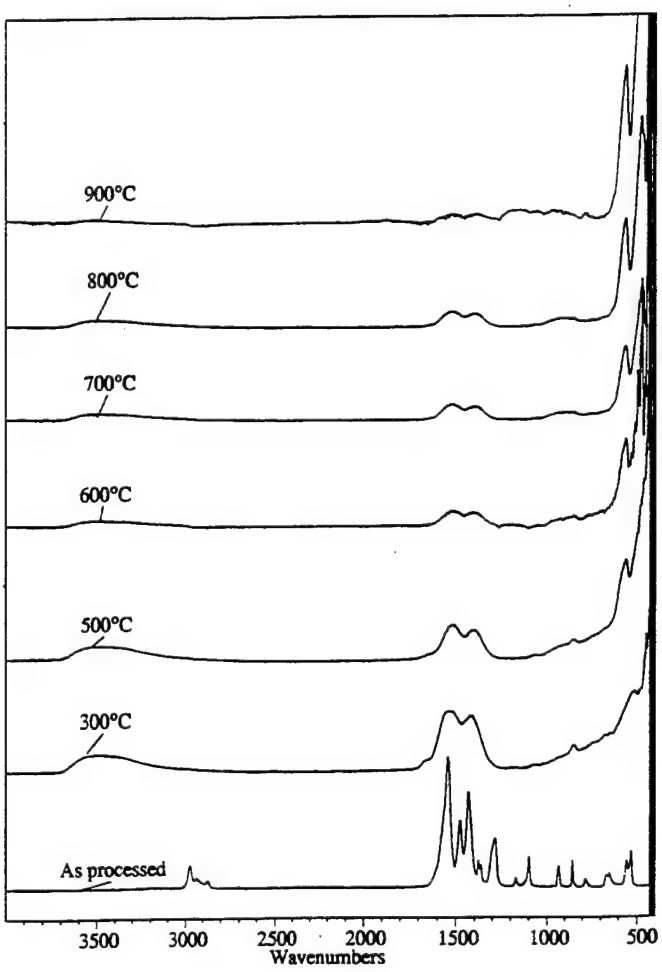

Figure 3.11: DRIFTS Spectra For Yttrium Isobutyrate Fired to Various Temperatures

X-Ray Powder Diffraction (XRD) Patterns: Figure 3.12 displays XRD powder patterns for Y-isobutyrate pyrolysis samples produced in the same manner as used in the DRIFTS studies. The absence of peaks in the 300°C sample indicates an amorphous material. At 500°C, bcc yttria begins to crystallize; however, the broad peaks and poor intensities suggest that considerable material is either amorphous or nanocrystalline. It is possible that the presence of a carbonate phase inhibits crystallization; although, no evidence exists to support this conjecture. Although most of the carbonate material has decomposed (by DRIFTS) by 800°C, and the remaining material is assumed to be stoichiometric Y_2O_3; the continued low intensities and broad peaks in the powder pattern still indicate a poorly crystalline material. Indeed, only by heating to 1400°C is a well defined pattern obtained with high relative peak intensities.

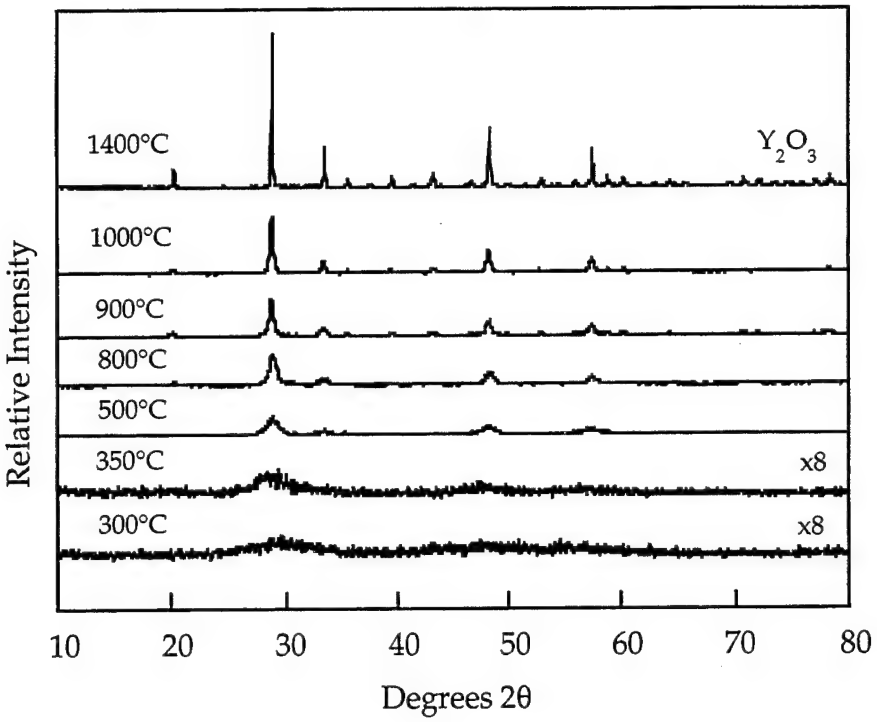

Figure 3.12: XRD Pattern of Yttrium Isobutyrate
Fired to Various Temperatures

3.2.2.5 Characterization of Precursor $3Y(O_2CCHMe_2)_3{:}5Al(O_2CCHMe_2)_3$: The YAG precursor was prepared by THF dissolution of the correct stoichiometric mixture followed by vacuum removal of solvent and grinding of the resulting powder as detailed in the experimental section. Samples of this bulk powder were then pyrolyzed to selected temperatures using the same procedures as used for the individual compounds.

Thermal analyses: Figure 3.13 TGA of the bulk, dry powder (5°C/min./air) appears to show a decomposition profile that is simply a superposition of both Al and Y isobutyrate decompositions. The initial mass loss would then correspond to partial hydrolytic decomposition of the Al fraction and the remaining major mass loss would then result from the primary decomposition of both types of isobutyrates. Indeed, the DTA shown in Figure 3.14 shows a small exotherm in the range 270-290°C that exactly parallels an event observed in the DTA for Al isobutyrate decomposition.

Because Figure 3.14 DTA, does not provide details about high temperature phase transformations (see discussion of Al isobutyrate DTA); fresh sample was first pyrolyzed to 500°C for 2 h, then identical amounts of sample and reference (20 mg each) were used to run the DTA at 5°C/min. to 1500°C to obtain the inset in Figure 3.14. The inset shows two exotherms in the range of 875-950°C. Although, the XRD data shown below (Figure 3.16) indicate formation of YAG alone, in the bulk samples; it is possible

that the first exotherm in the DTA corresponds to initial crystallization of some delta-alumina followed by reaction with yttria and subsequent crystallization of the YAG phase. As discussed in the following sections, yttria, which begins to crystallize at 500°C in the bulk decomposition studies is not seen in the mixture; thus, the exact nature of the observed thermal events remains in question.

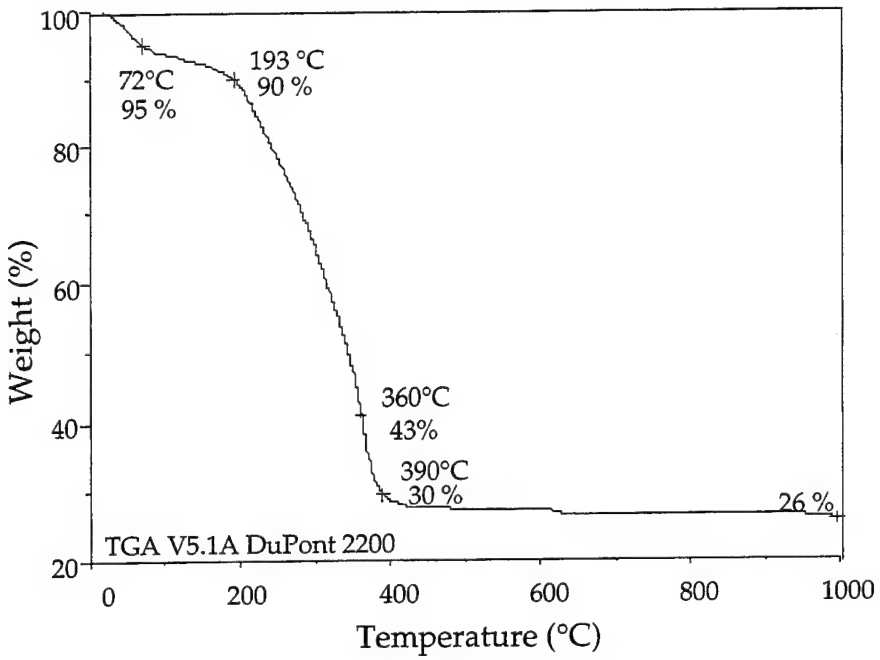

Figure 3.13: TGA of YAG Isobutyrate Precursor

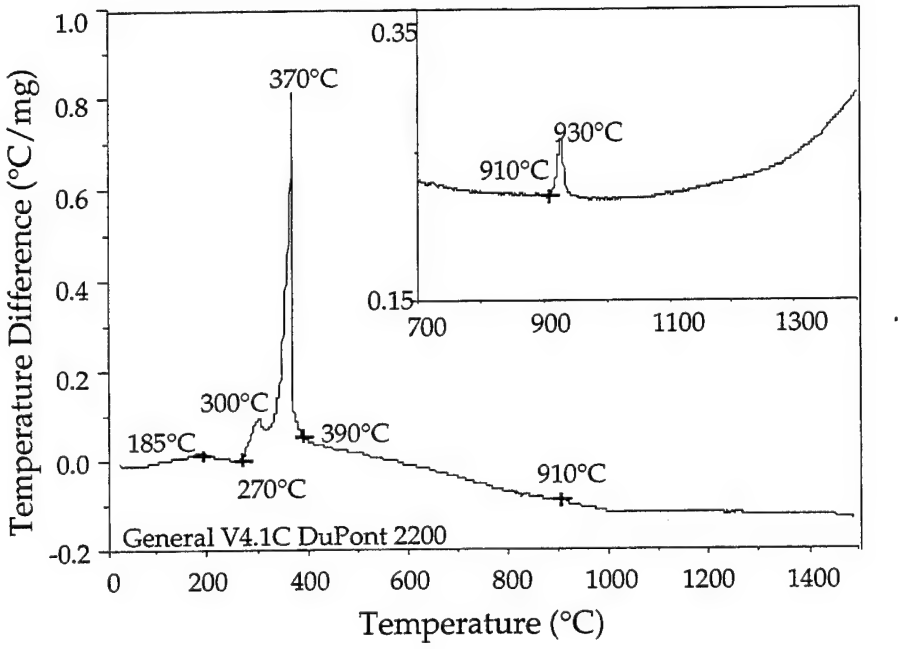

Figure 3.14: DTA of YAG Isobutyrate Precursor

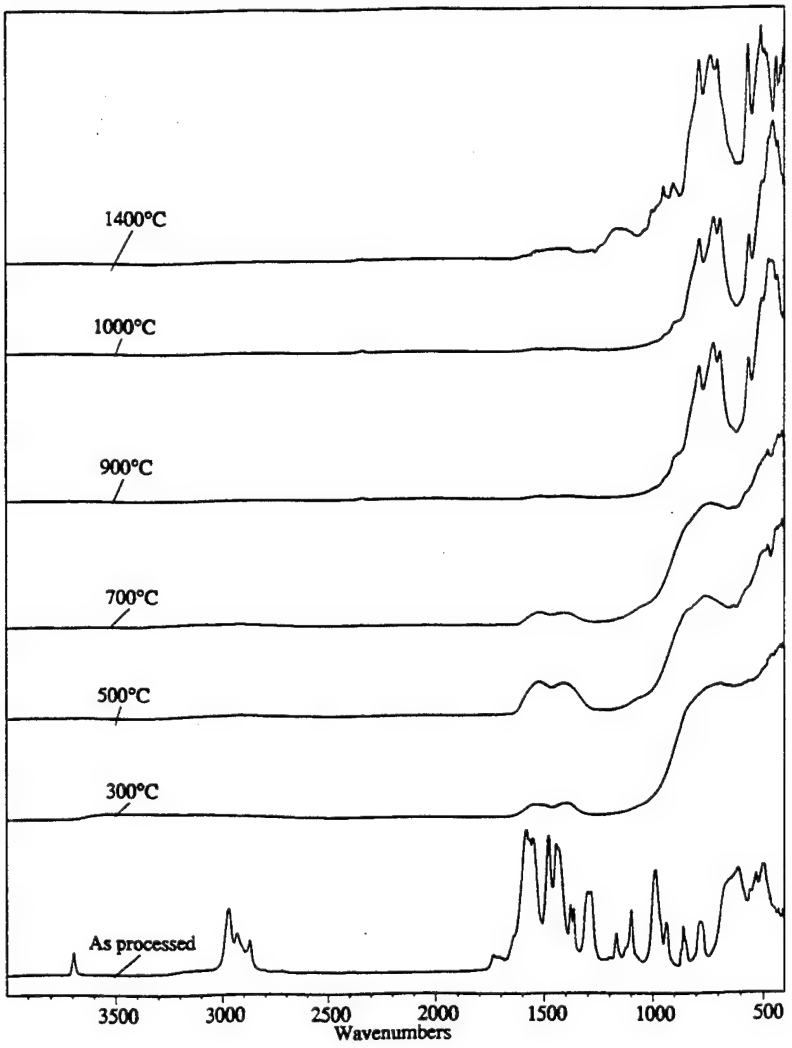

Figure 3.15: DRIFTS Spectra of YAG Isobutyrate Precursor Fired to Various Temperatures

DRIFTS: Spectra of as-processed YAG precursor, and precursor heated to selected temperatures are shown in Figure 3.15. The IR spectrum of as-processed YAG precursor looks like an overlap spectrum constructed from IR spectra of the Y and Al isobutyrates. Again, it appears that no significant intermolecular interactions occur when the Y and Al isobutyrate are mixed in solution. The IR spectra of the as-prepared YAG precursor shows peaks at: 3690 cm^{-1} (nAlO-H); 2932, 2872, and 2871 cm^{-1} (nC-H), and at 1583, 1559, 1477, 1442, and 1433 cm^{-1}(nC=O).

However, on pyrolysis, the resulting materials do not behave as the individual isobutyrates. At 300°C, all of the organic ligand peaks disappear to be replaced by carbonate peaks centered at 1530 and 1400 cm^{-1}. A barely detectable nO-H peak is observed in the 300°C spectrum but not at higher temperatures. The carbonate peaks persist to only 700°C; however, no evidence is found at low temperatures for a sharp nY-O peak at 560 cm^{-1} which is corroborated by the lack of an yttria bcc pattern in the

XRD studies. In addition, a broad peak at 650-1000 cm^{-1} is found in the 300 through 700°C spectra. This peak, which eventually evolves into four peaks at 560, 690, 720 and 790 cm^{-1} at 900°C and above, is not found in spectra of Al isobutyrate or Y isobutyrate samples heated to the same temperatures. These four peaks correspond to the formation of crystalline YAG.[22] These observations when coupled with t the following XRD data, strongly suggest that some novel intermolecular chemical bonding does occur in the unpyrolyzed YAG precursor that is different from that in individual Y or Al isobutyrates. This bonding must play a role, at the atomic level, in the exclusive formation of the YAG phase.

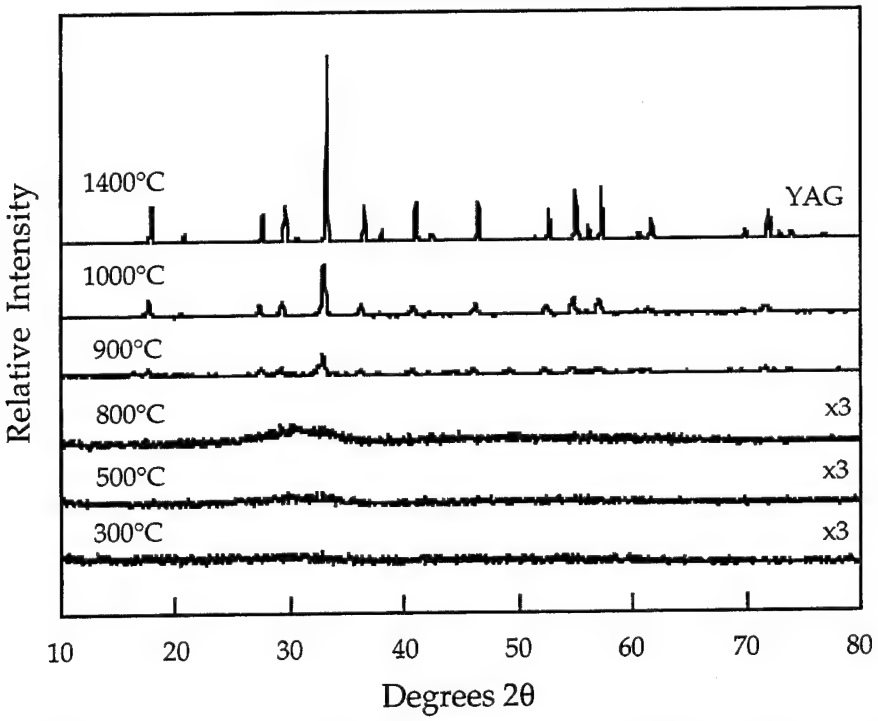

Figure 3.16: XRD Pattern of YAG Isobutyrate Precursor Fired to Various Temperatures

X-Ray Powder Diffraction Patterns: XRD patterns of the DRIFTS pyrolysis samples are shown in Figure 3.16. No intermediate crystalline phases such as Y_2O_3, delta- and alpha-alumina are observed before crystallization of YAG, which starts at about 875°C (from DTA data). Above 900°C, YAG continues to crystallize as evidenced by continued refinement in peak shapes and intensities. The simplicity of the observed XRD patterns is at odds with what is observed in the individual precursor pyrolysis studies, i.e.. given that in the Y isobutyrate pyrolysis, Y_2O_3 crystallization starts at 500°C. These results strongly support our contention that good atomic mixing is obtained through the use of carboxylate precursors and that the formation of a multimetallic isobutyrate complex may partly account for the unique processing differences observed.

3.2.2.6 YAG Fiber Processing from Isobutyrates: Figure 3.17 a) is an SEM micrograph of an extruded green fiber. The as-spun fiber has a circular cross-section, a smooth surface and is 70 μm in diameter. After heating above 100°C, the fibers begin to crack (Figure 3.17 b)). For large diameter fibers (> 20 μm), cracking occurs even with extremely slow heating. Crack-free fibers could not be prepared even after extensive studies of heating schedules. However, fine diameter fibers can be easily heated without damage. It is necessary to keep the fiber diameter finer than 20 μm to avoid this cracking.

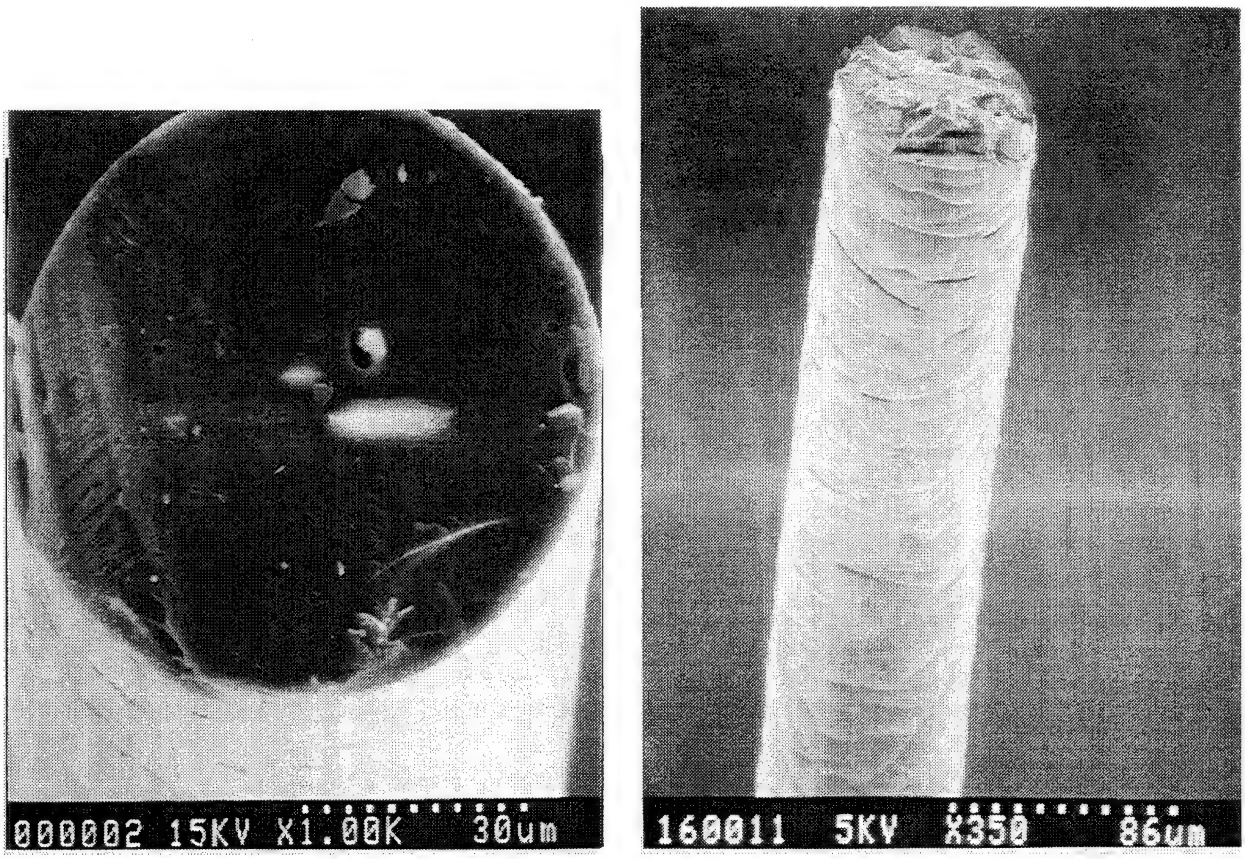

a) b)

Figure 3.17: Isobutyrate-Derived YAG Fibers a) As Spun, b) After Heating Above 100°C

The isobutyrate fibers have unusual sintering behavior. If they are heated rapidly to 1500°C (15°C/min.), they produce nearly dense YAG fibers. The microstructure of a rapidly heated isobutyrate fiber appears in Figure 3.18 a). The YAG grain size is about 1000 nm. Contrast this with Figure 3.18 b), the microstructure of a similar isobutyrate fiber heated to 1500°C with a very slow heating rate (0.5°C/min. near 900°C). This material is much more porous. Many YAG grains have a coordination number of 2 or 3. The YAG grain size is 500-1500 nm with many interconnected 500-1000 nm pores, nearly as large as the grains, a classical "unsinterable" microstructure. This curious effect of heating rate, also seen with the formoacetates, is not understood.

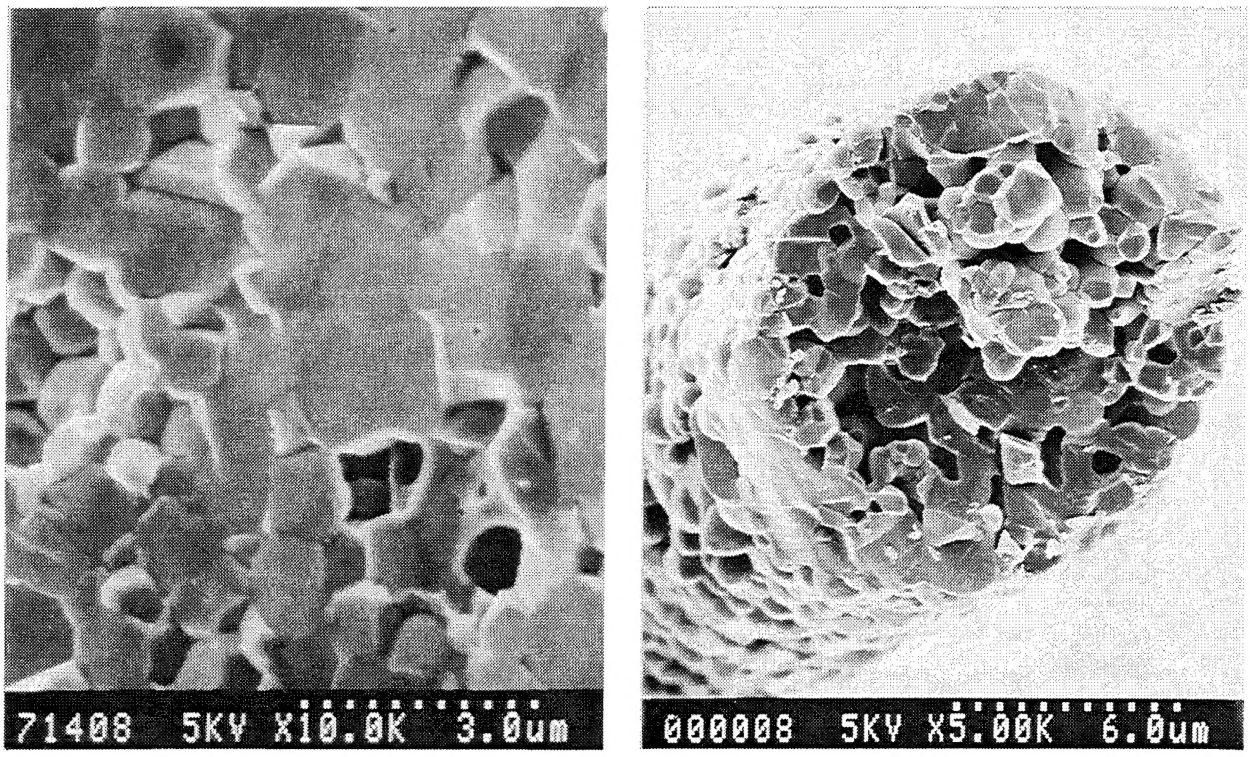

a) b)

Figure 3.18: Isobutyrate-Derived YAG Fibers Fired to 1500°C. a) Rapid Ramp and b) Slow Ramp

3.3 Conclusions of Carboxylate Precursors for YAG Fibers

Dense, fine diameter YAG fibers can be prepared from carboxylate precursors, using aqueous formoacetate solutions and THF-based isobutyrate solutions. Both systems are readily spinnable. Upon pyrolysis, they undergo a series of reactions, leading to crystallization of the YAG phase at 900°C. Phase-pure YAG is readily obtained from both systems. The synthesis and pyrolytic transformations of the isobutyrate system has been characterized in some detail.

Dense, defect-free YAG fibers can be obtained in both systems, provided that the green fiber diameter is finer than about 20 μm and the pyrolysis is conducted appropriately. Coarser diameter isobutyrate fibers crack during the early stages of heating. Coarse formoacetate fibers bloat, crack, or become hollow. Inappropriate sintering can lead to very porous YAG fiber, often with a large central void. Effective pyrolysis schedules were identified for both systems, featuring relatively rapid heating (15°-25°C/min.) between 900°C and 1500°C.

REFERENCES

1. G.S. Corman. "High Temperature Creep of Some Single Crystal Oxides." *Ceram. Eng. and Sci. Proc.*, **12** [9-10] 1745-1767 (1991)

2. (a) T.A. Parthasarathy, T. Mah, and K. Keller. "High Temperature Deformation Behavior of Polycrystalline Yttrium Aluminum Garnet (YAG)." *Ceram. Eng. and Sci. Proc.*, **12** [9-10] 1767-1773 (1991)
(b) J. Wolfenstine and T.A. Parthasarathy. "Elevated Temperature Deformation of a Fine-Grained $Y_3Al_5O_{12}$+$YAlO_3$ (20 vol.%) Material." *Scripta Metallurgica et Materialia*, **26** 1649-1653 (1992)

3. J.W. Pugh. *Met. Trans.*, **4** 553f-538 (1973)

4. E. Pink and L.Barha, ed. *The Metallurgy of Doped Non-Sag Tungsten*, Elsiever, London, (1989)

5. A. Ziabicki. *Fundamentals of Fiber Formation*. p. 367-373,Wiley-Interscience, New York, (1976)

6. (a) G. Gowda. "Synthesis of yttrium aluminates by the sol-gel process." *J. Mat. Sci. Lett.*, **5** 1029-1032 (1986)
(b) R.S. Hay, E.E. Hermes, and K.A. Jepsen. "Microstructure and Phase Evolution in Sol-Gel Derived YAG Thin Films." *Ceramic Transactions-Ceramic Thin and Thick Films*, edited by B.V. Hiremath. Vol. 11, p.243

7. A. Ziabicki. *Fundamentals of Fiber Formation*, p. 13,Wiley-Interscience, New York, (1976)

8. E.B. Bagley and H.P. Schreiber. *Transactions of the Rheological Society*, **5** 341 (1961)

9. (a) Gregory N. Morscher and Haluk Sayir. "Thermomechanical Bend Properties of Single Crystal and Polycrystalline Alumina-Based Fibers." *16th Conference on Metal Matrix, Carbon and Ceramic Matrix Composites Proceedings*. NASA CP 3175. 657-676
(b) William B. Hillig. "A New Model for Testing Fiber Failure Strain." *Am. Cer. Soc. Bull.*, **66** [2] 373-376 (1987)
(c) P.A. Siemers, R.L. Mehan and H. Moran. "A Comparison of the Uniaxial Tensile and Pure Bending Strength of SiC Filaments." *J. Mat. Sci.*, **23** 1329-1333 (1989)

10. (a) Sybrand van der Zwaag. "The Concept of Filament Strength and Weibull Modulus." *Journal of Testing and Evaluation*, **17** [5] 292-298 (1989)
(b) Daniel R. Roberts, Enrique Cuellar, Michael T. Kennedy and John E. Ritter, Jr. "Calculation of Static Fatigue Lifetime of Optical Fiber." *Optical Engineering*, **30** [6] 716-727 (1991)

11. M.A. Leitheiser and D.M. Wilson. "Advanced Fiber Development and Characterization: Volume IV - Alumina Fiber Development." NASP Contractor Report 1129, Vol. IV. Contract F33657-87-C-2214. November 1991.

12. G.N. Morscher, J.A. DiCarlo, and T. Wagner. "Fiber Creep Evaluation by Stress Relaxation Measurements." *Ceram. Eng. and Sci. Proc.*, **12** [7-8] (1991)

13. R.M. Laine, K.A. Youngdahl, R.A. Kennish, M.L. Hoppe, Z.-F. Zhang and D.J. Ray. "Superconducting Fibers from Anhydrous Metal Carboxylates." in *Better Ceramics Through Chemistry IV, Mat. Res. Symp. Proc.* Vol. **180**, B.J. Zelinski, C.J. Brinker, D.E. Clark, and D.R. Ulrich eds. (1990) p. 865

14. E. Wood and D.M. Wilson. "Microcrystalline Ceramic Articles." U.S. Patent 4,954,462, September 4, 1990

15. a) H.G. Sowman, "Alumina-Boria-Silica Ceramic Fibers from the Sol-Gel Process." Chapter 8 in *Sol-Gel Technology for Thin Films, Fibers, Preforms, Electronics, and Speciality Shapes*. L.C. Klein, ed. Noyes Publications, Park Ridge NJ, (1988)
b) E.A. Richards, C.J. Goodbrake, and H.G. Sowman. "Reactions and Microstructure Development in Mullite Fibers." *J. Am. Ceram. Soc.*, **74** [10] 2404-2409 (1991)

16. a) N.M. Chaplygina and S.M. Portnova. "The $Y(HCOO)_3$-HCOOH-H_2O System at 50°C." *Russian Journal of Inorganic Chemistry*, **30** [1] 125-127 (1985)
b) N.M. Chaplygina, I.Z. Babievskaya, and N.I. Ivanov, "The $Al(HCOO)_3$-HCOOH-H_2O System at 50°C." *Russian Journal of Inorganic Chemistry*, **30** [8] 1218-1219 (1985)
c) N.M. Chaplygina, I.Z. Bagievskaya, and I.B. Kudinov. "Preparation and Physicochemical Properties of $Al(HCOO)_3{:}3H_2O$." *Russian Journal of Inorganic Chemistry*, **29** [9] 1260-1263 (1984)

17. Y. Masuda. "Thermal Decompositions of Formates. Part VII. Thermal Decomposition of Yttrium Formate Hydrate." *Thermochimica Acta*, **53** 215-223 (1982)

18. V.N. Maksimov, K.N. Semenko, T.N. Naumova, and A.V. Novoselova. "The Aluminum Acetates." *Russian Journal of Inorganic Chemistry*, **5** [3] 276-270 (1960)

19. a) W.M. Carty, G.C. Stangle, R.M. Laine, K. A. Youngdahl. *SAMPE Quart.*, Oct. (1988) p. 3
b) R.M. Laine, K.A. Youngdahl, R.A. Kennish, M.L. Hoppe, Z-F. Zhang, D.J. Ray. "Superconducting Fibers from Organometallic Precursors, Part II: Chemistry and Low Temperature Processing." *J. Mater. Res.*, **6** 895 (1991)
c) R.M. Laine, K.A. Youngdahl. U.S. Patent 5,071,833, 1993

20. Yin Liu, Zhi-Fan Zhang, Bruce King, John Halloran, and Richard M. Laine. "Synthesis of Yttrium Aluminum Garnet Using Isobutyrate Precursors." *J. Am.*

Ceram. Soc., in press

21. L.M. Seaverson, S.W. Lou, P.L. Chien, and J.F. McClelland. "Carbonate Associated with Hydroxide Sol-Gel Processing of Yttria: A Spectroscopic Study." *J. Am. Ceram. Soc.*, **69** 423-29 (1986)

22. P. Apte, H. Burke, H. Pickup. "Synthesis of Yttrium Aluminum Garnet by Reverse Strike." *J. Mat. Sci.*, **7** 706-711 (1992)